ELECTROOSOMOTIC FLOW IN TEMPLATE PREPARED CARBON NANOTUBES

By

WILLIAM C. HARDY

A THESIS PRESENTED TO THE GRADUATE SCHOOL
OF THE UNIVERSITY OF FLORIDA IN PARTIAL FULFILLMENT
OF THE REQUIREMENTS FOR THE DEGREE OF
MASTER OF SCIENCE

UNIVERSITY OF FLORIDA

2011

To my parents, my brother, my lab associates and God Almighty

ACKNOWLEDGMENTS

My graduate years at the University of Florida have had mentorship from numerous outstanding individuals both from within the university and outside of it. It is to these individuals, whom have invested time, support and insight to my studies, which my heartfelt gratitude and thanks go out to, for without their help, this thesis would not have been possible.

I would like to thank Dr. Charles R. Martin for his patience, guidance, support, and encouragement throughout my graduate career at the University of Florida. He has been an excellent mentor by providing scientific discussion, suggestions, knowledge about my research, and constructive criticism about how to more effectively communicate science. His dedication from the initial to the final stage has enabled me to develop a substantial understanding of electrochemistry and fluid dynamics.

The Martin group members have been very supportive. I am especially grateful to Jillian Perry, Lloyd Horne, Greg Bishop, Hitomi Mukaibo, Dooho Park, Kaan Kececi, Pu Jing, Fonda Tongay, and Otoyne Braide, for providing insightful discussions about my experiments, and for valuable training in surface modification, analytical detection techniques and instrumentation. Li Zhao, Lindsey Sexton, and Marcos Lopez shared their research experiences and provided helpful experimental method suggestions.

I want to thank Dr. David Wei, Dr. Rick Yost, Dr. Danyell Wilson, and Dr. Anne Donnelly for their valued advice on my research, life, and career. I am also grateful to Karen Kelly and Kim from the ICBR for their help with SEM and TEM, to Eric Lambers from the MAIC for his help with XPS, and Dr. Reynold’s and his group for their help with the four point probe measurements.

Finally, my gratitude goes to my family and friends who provided enormous help and moral support during my graduate career. My parents Lathen and Katherine Hardy Jr., and my brother Lathen Hardy, III deserve most of the credit for my success as they were constant sources of encouragement and guidance before and during my graduate career. I want to also thank members of the Black Graduate Student Organization and the Office of Minority Programs, especially Dr. Lawerence Alexander, Sarah Cuningham and Janet Broiles for providing a very friendly, atmosphere and helping me make the transition from Jackson, Mississippi to Gainesville, Florida smooth.

Lastly, I offer my regards and blessings to all of those who supported me in any respect during the completion of this project.

TABLE OF CONTENTS

page

LIST OF TABLES

LIST OF FIGURES

LIST OF ABBREVIATIONS

CNM	carbon nanopore membrane
CNT	carbon nanotubes
EOF	electroosmotic flow
LIB	lithium ion batteries
SEM	scanning electron microscopy
TEM	transmission electron microscopy
XPS	x-ray photoelectric spectroscopy

Abstract of Thesis Presented to the Graduate School
of the University of Florida in Partial Fulfillment of the
Requirements for the Degree of Master of Science

ELECTROOSOMOTIC FLOW IN TEMPLATE PREPARED CARBON NANOTUBES

By

William Hardy

December 2011

Chair: Charles R. Martin
Major Chemistry

The fabrication of carbon nanotube membranes (CNMs) is an area of emerging research. The strength, small dimensions and the remarkable physical properties of carbon nanotubes have made them a material with a wide range of promising applications. Many of these applications will require the use of uniform dense arrays of free-standing, open-ended nanotubes. In the research presented in this thesis, CNMs are prepared by template synthesis. Template synthesis entails chemical vapor deposition of ethylene gas onto a commercial alumina membrane. By utilizing this method carbon nanotubes can be grown with tailored properties, dimensions, and shapes.

The objective of this research was to customize the chemical, physical, and structural properties of carbon nanotube membranes and to study the fundamental transport processes occurring at the interface of the carbon nanotube membranes and the electrolyte by monitoring and controlling electroosmotic flow.

In Chapter 2, we describe the utilization of the template method to fabricate carbon nanotube membranes. This method involves the synthesis of carbon nanotube membranes by chemical vapor deposition within the pores of high pore density alumina

membrane templates. We thoroughly explain the advantage of using template synthesis to customize nanostructures with specific characteristics. We demonstrate that by controlling the parameters of chemical vapor deposition, we can tune the properties of the carbon nanotube membrane. Lastly, we discuss the methods of characterization for the CNM.

In Chapter 3, we describe EOF in carbon nanotube array membranes. EOF was driven across the CNM by placing the membrane between two electrolyte solutions and placing an electrode in each solution to pass a constant current through the nanochannels of the membrane. EOF was monitored by measuring the flux of a probe molecule across the membrane. The CNMs have an anionic surface charge, which results in EOF in the direction of cation migration across the membrane. EOF was used to control the flux of the probe molecule. When EOF was driven in the direction of diffusion there was an increase in the flux of the probe molecule across the membrane. Reversing EOF decreases flux, and at high reverse EOF velocities the transport is halted and eventually produces transport in the opposite direction. EOF through the CNM was modified by changing the pH, ionic strength and the current density applied to the membrane. These changes resulted in the exhibited control of EOF velocity and direction. Results from this work will lay a solid foundation for the further development of selective molecular transport in CNMs.

CHAPTER 1
INTRODUCTION AND BACKGROUND

Energy storage is more vital today than at any other time in human history. Applications such as low emission hybrid electric vehicles, portable electronic devices (cell phones, laptop computers etc.), and the need for power storage from renewable sources put even more stringent requirements on energy storage devices.[1]

In all of the applications mentioned above, high performance batteries can be applied. Rechargeable lithium ion batteries have become the dominant power source choice for the fulfillment of such energy demands.

The first prototypes of lithium batteries used Li-metal as the anode material. The motivation for producing a battery technology based on Li-metal as an anode was based on the fact that lithium is the most electropositive (–3.04 V versus standard hydrogen electrode) and the lightest (equivalent weight M = 6.94 g mol^{-1}, specific gravity ρ = 0.53 g cm^{-3}) metal, which promotes the design of storage systems with very high energy density. [1-2]

These first lithium based batteries were unsuccessful because Li-metal is highly unstable and led to many safety concerns. Thus, Sony ® in 1991 decided to use lithium ion moving electrodes instead of lithium metal in their rechargeable battery design. Although the Li-ion battery is slightly lower in energy density, it is much safer and offers considerable environmental value. (Oxidized lithium ions are non-toxic. They can easily be extracted from a battery, neutralized, and used as feedstock for new Li-ion batteries.)

For these purposes intensive research efforts have been directed at creating both efficient and safe lithium ion cells by many universities, government agencies, and battery companies. However, some problems still have to be solved before the

complete success of the lithium ion battery is achieved. Among the concerns are long-term stability of cell components, heat control of the cell, higher quality product development, and better cost-performance of materials.

General Concept of a Battery

A battery consists of a group of interconnected electrochemical cells. The quantity of cells grouped together and the method by which they are connected depends on the specific application for which the battery is designed. An electrochemical cell is composed of a negative electrode (anode), a positive electrode (cathode) and an electrolyte. These components are the essential building blocks of any battery.[4-5]

Electric energy is released or discharged from a battery when it is connected to a work load. The anode reacts with the ions in the electrolyte and releases electrons through an oxidation reaction while the cathode reacts with the ions in the electrolyte and incorporates electrons through a reduction reaction. When these reactions are reversible, the battery is a rechargeable battery, meaning the electric energy is restored or charged when the battery is connected to an external power supply and the opposite reactions are induced. The energy density of an electrode is defined by the amount of electrons that can be stored per unit volume or weight. [1, 4]

The anode of a lithium ion cell is usually a solid reductant and the cathode is usually a solid oxidant. A typical lithium ion cell used today is commonly composed of a carbon-based material as the anode and a lithiated transition metal oxide as the cathode.

During the charge cycle of the cell, the cathode material releases Li ions to the electrolyte (deintercalation) and electrons are removed from the cathode by an external field and transferred to the anode. Li ions then rush to the carbon based anode to

compensate for the charge- (intercalation). The chemical reactions at the anode and cathode of a Li-ion cell are reversible. On discharge, the anode supplies intercalated Li ions to the electrolyte and electrons to the external circuit, the cathode is an electronically conducting medium into which the Li ions intercalate from the electrolyte and compensate for the charge of the electrons from the external circuit. Since both anode and cathode are hosts for the reversible intercalation/deintercalation of Li ions from/into the electrolyte, the cell is known as a “rocking-chair” electrochemical cell.[4-5]

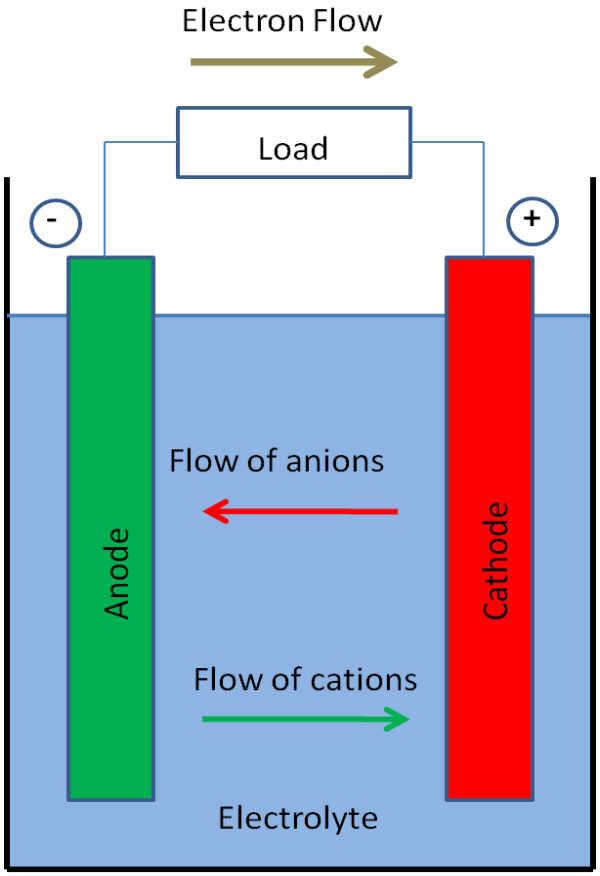

Figure 1-1. Schematic representation of a general electrochemical battery cell Li- Ion batteries

Although different applications have different requirements, the most common carbon material for the anode is either graphite, coke type, or a combination of both. Common cathode materials include $LiMn_2O_4$, $LiCoO_2$ and $LiNiO_2$. Electrolyte can be

either liquid or solid. Liquid electrolyte is usually a non-aqueous solution of a lithium salt and various solvents including different types of esters, ethers and carbonates. A schematic of a typical Li-ion cell is shown in Figure 1-2[5] and the general reactions taking place at the electrodes in a Li-ion cell are depicted in Figure 1-3.

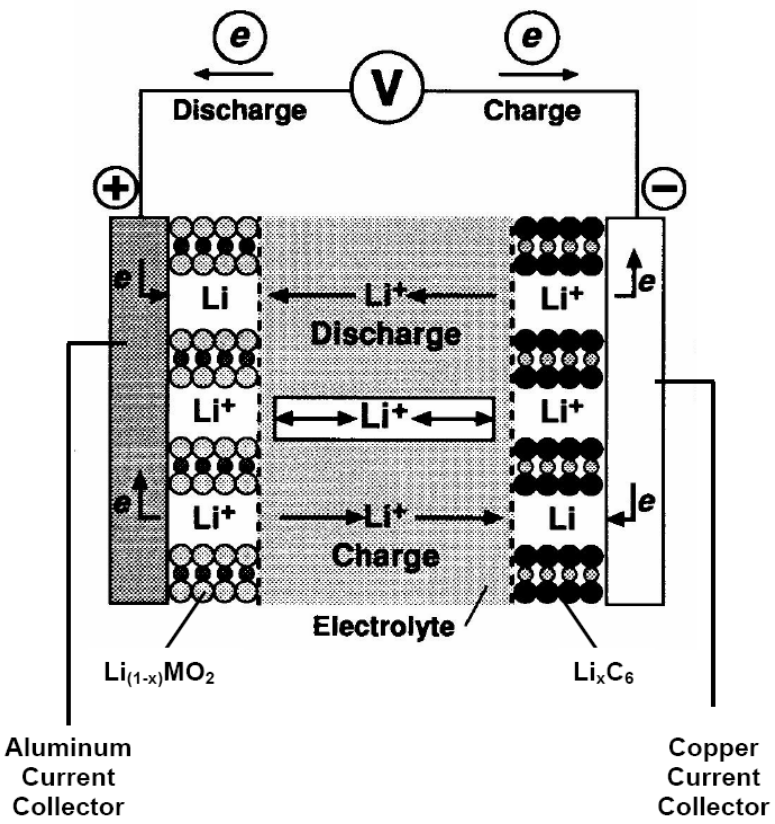

Figure 1-2. Schematic representation of the charge-discharge process of a lithium ion cell

The lithium ion battery has shown superior characteristics in both energy density and cell voltage when compared to other battery systems. These advantages have given lithium ion batteries success in the small application market and a great deal of interest in possible large scale applications.

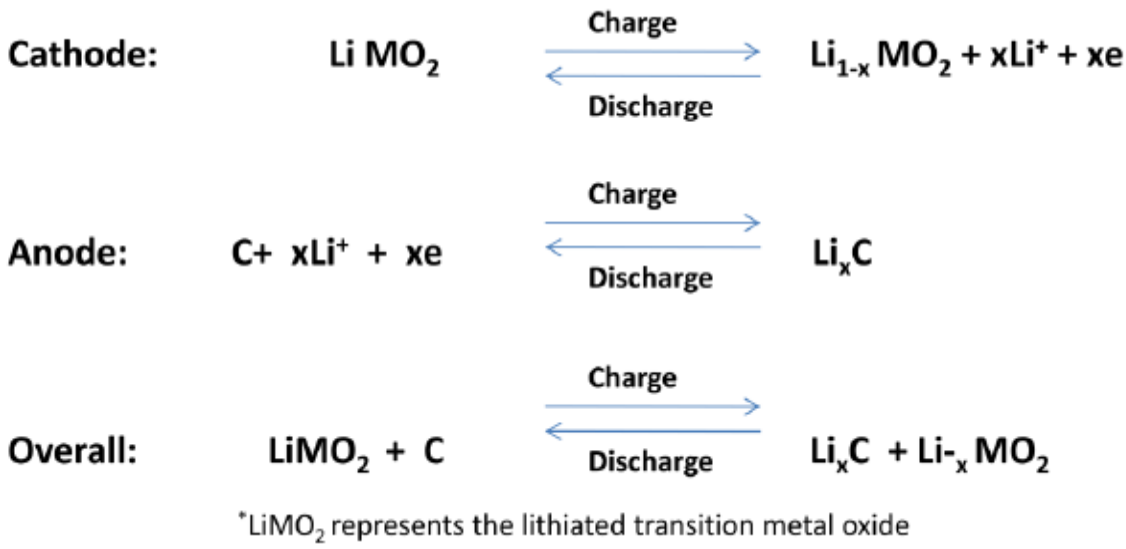

Figure 1-3. The general reactions taking place at the electrodes and the overall reaction for a typical Li ion cell

Battery Separators

As stated earlier, rechargeable lithium ion batteries have achieved a great deal of commercial success and established dominance in small cell applications. Their high energy density and intrinsic discharge voltage also make them desirable candidates for larger applications, including electronic vehicles and satellites.[6-7]

Such applications require a higher performance standard for lithium ion batteries. An ideal battery would be reliable, robust, and inexpensive. It would supply a constant power supply under heavy loads and at high and low temperatures. It would be safe under critical environmental conditions and be easy to mass produce.[6-8]

One way to universally improve lithium ion battery performance is through the use of advanced battery separators. A battery separator is a porous membrane placed between the anode and cathode of a battery. The main function of a separator is to keep the positive and negative electrodes apart in order to prevent electrical short

circuits, while also allowing the transport of ionic charge carriers which are needed to complete the circuit during the passage of current in an electrochemical cell.[9-10]

Figure 1-4. Structure of Lithium-Ion battery with battery separator

Separators have been manufactured using a variety of different materials including cellulosic papers, cellophane, nonwoven fabrics, foams, ion exchange membranes, and micro-porous flat sheet membranes made from polymeric materials. As batteries have become more complex, separator function has also become more demanding, sophisticated and multifaceted.[10-11]

There are many properties that are required for separators used in electrochemical batteries. Battery separators should be good electronic insulators, have the ability to conduct ions by either ionic conduction or by soaking electrolyte, and minimize any processes or reactions that adversely affect the electrochemical energy efficiency of the batteries.[9]

Relative to the amount of research on electrode materials and electrolytes, very little attention has been aimed at characterizing and developing new separators. Likewise, there has been modest interest given to separators in publications reviewing battery technologies. In recent years there have been numerous reviews on battery cell

fabrication, their performance, and application in real life applications, but very few reviews have discussed separators in detail.[9-19]

The majority of the separators currently used in batteries were originally designed for applications in other existing technologies. They were usually not developed specifically for the batteries in which they are utilized and thus there is a need for optimization.[8, 20-21]

The research results presented in this thesis have been aimed at studying the transport processes occurring at the interface of a porous carbon nanotube membrane and an electrolyte through different electrochemical approaches. The carbon nanotube membrane is synthesized using the template method. The advantage of this approach is the structural, physical, and chemical properties of the carbon nanotube membrane can be modified through stringent control of the experimental parameters of the chemical vapor deposition of carbon. The flexibility of the template method will enable these membranes to exhibit optimized permeability and selectivity. The results from this research should also be helpful in the practical application of using a carbon nanotube membrane as a possible new material for advance battery separators.

Carbon Nanotubes

The discovery of carbon nanotubes was credited to Sumio Iijima in 1991. Iijima was studying the structure of buckmisterfullerenes created by the arc-discharge process, when he noticed an extremely thin needle like material observed under an electron microscope. The material proved to be graphite in structure and was a few hundred nanometers in length so he called the material, carbon nanotubes. [22-23]

Carbon nanotubes can generally be described as a graphite sheet rolled up into a nanoscale-tube. There are several types of nanotubes; but they can be divided in two

main categories: single walled carbon nanotubes (SWCNTs), and multi-wall carbon nanotubes (MWCNTs).

Single-walled carbon nanotubes (SWCNT) typically have a diameter of about 1 nanometer, with a tube length that can be many millions of times longer. The structure of a SWNT can be conceptualized as one-atom-thick layer of graphite called graphene wrapped into a seamless cylinder. SWCNTs are often considered to be structurally perfect because of the high structural order that they possess. [22-23]

Multi-walled carbon nanotubes (MWCNT) consist of multiple rolled layers of concentric tubes of graphite. MWCNT can be conceptualized using the Parchment model. In the Parchment model, a single sheet of graphite is rolled around itself, resembling a scroll of parchment or a rolled newspaper. The interlayer distance in multi-walled nanotubes is close to the distance between graphene layers in graphite, which is approximately 3.4 Å. MWCNTs are generally prepared with different levels of graphitization which means MWCNTs are typically less ordered than SWCNTs. [22]

Carbon Properties

The physical properties of carbon nanotubes are still being discovered and disputed. CNTs have a broad range of electric, thermal, and structural properties that change depending on the dimensions and unique structure of the nanotube.

Many studies have confirmed that the sp^2 carbon-carbon bonds in CNTs supply amazing mechanical properties to the structure of the nanotube. The stiffness of a material is measured in terms of its Young's modulus, which is the rate of change of stress with applied strain. The Young's modulus of CNTs can be as high as 1000 GPa which is approximately 5x higher than steel. The tensile strength, or breaking strain of CNTs can be up to 63 GPa, which is about 50x higher than steel. Research has also

indicated that CNTs are considered to be great conductors of heat and may someday find applications as miniature heat conduits in a host of devices and materials. [24-27]

The electronic properties of carbon nanotubes are also extraordinary. The fact that CNTs can be metallic or semiconducting depending on their structure is particularly remarkable. Thus, some CNTs have conductivities higher than that of copper, while others behave more like silicon. There is great interest in the possibility of constructing nanoscale electronic devices from CNTs, and some progress is being made in this area. However, in order to construct a useful device we need to arrange many thousands of CNTs in a defined pattern. [28-30]

Carbon Nanotube Synthesis

Carbon nanotubes are commonly produced by three main techniques, laser ablation, arc discharge and chemical vapor deposition. In the laser ablation technique, a high-power laser beam impinges on a volume of carbon, while simultaneously an inert carrier gas is bled though the chamber. Nanotubes subsequently develop on the cooler surfaces of the reactor as the vaporized carbon condenses. In the arc discharge technique, a direct electrical current is applied between two carbon electrodes in a gas atmosphere. As the high energy current passes between the carbon electrodes a carbon vapor is produced. Carbon nanotubes can self-assemble from the resulting vapor with or without a catalyst. [22, 31-35]

Both of these techniques can produce high quality nanotubes, but producing large quantities of uniform high purity carbon nanotubes is still an arduous task. Using these techniques, to grow large amounts of CNTs typically produces low quality masses of CNTs that are randomly mixed with a variety of by-products. High purity SWCNTs are produced on a small scale but they are moderately expensive. MWCNTs are

synthesized on the large scale but size uniformity is difficult to control using these techniques. [36-37]

Chemical Vapor Deposition (CVD) is a process in which precursor gases typically diluted in carrier gases are introduced into a reaction chamber at ambient temperatures. As the gas comes into contact with a heated substrate, a reaction takes place causing the decomposition of the source gas which forms a solid phase. This solid phase is preferentially deposited onto the substrate. The substrate temperature is a critical parameter, which can influence what reactions will take place. [38]

CVD has several advantages over other methods. First, the CVD method allows opportunities to easily control the growth of CNTs which is an option not readily available in the laser ablation or arc discharge methods. Second, the CVD is a method that is easily scaled up for mass production of CNTs. Third, because in CVD the gas flows in a certain direction the nanotubes that are grown are anchored to the substrate material at one end, which allows for directional, aligned growth controlled strategies. These strategies can include controlling gas flow rate, van der Waals interactions, and electric fields. Lastly the CVD method is easily manipulated and is highly compatible with the template synthesis method for fabricating controlled arrays of nanostructures. [36, 39-47]

Template Synthesis Method

The Martin laboratory and others have illustrated the versatility of this method by growing carbon nanotubes by CVD along the outer surface and inner pore walls of nanoporous templates. This method has resulted in films of high density, free standing defect-free arrays of carbon nanotubes embedded in the pores of the template. [48-52]

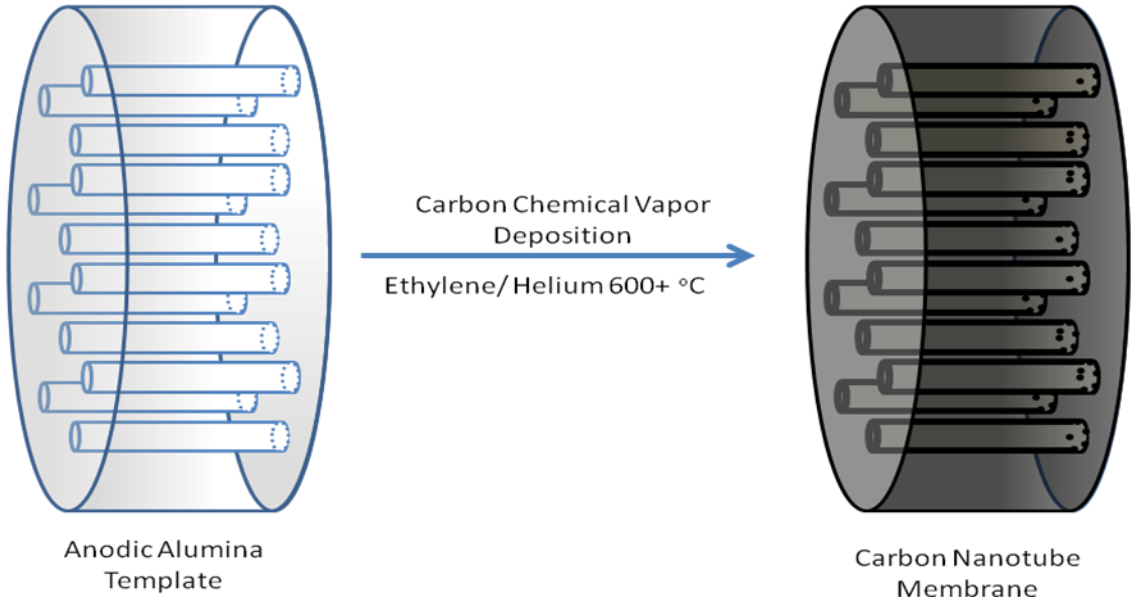

Figure 1-5. Chemical vapor deposition of carbon onto the anodic alumina membrane

The template synthesis method is a technique for preparing one-dimensional nanostructures. The Martin group pioneered this method in the late 1980s and early 1990s, [47, 53-54] although the method originated with Possin[55] who applied it for the fabrication of metal nanowires. In the template method, a material is deposited into the pores of a mask called the template. Typically this deposition results in mono-dispersed arrays of dense parallel nanostructures in the shapes and dimensions of the predisposed template pores. By controlling the deposition conditions, one can vary the wall thickness and thus produce hollow or solid nanostructures.

The template synthesis method is a universal technique for producing nanostructures with various geometries and dimensions composed of a variety of different materials[46-47, 56-59.] It has been used to produce nanowires, nanotubes, nanopillars, and even drug molecular vehicles. The broad utility of this method is illustrated by considering the examples of fabrication of biodegradable nano test tubes for drug delivery[60] and conducting polymer nanostructures for energy storage[61].

Anodic Aluminum Oxide Template Membranes

Anodic aluminum oxide (AAO) nanoporous membranes (Figure 1-5) are used as the templates for the carbon nanotube membranes discussed in this thesis[51, 62.] AAO membranes are inorganic films composed of a high purity alumina matrix manufactured electrochemically. AAO membranes make remarkable templates for this project for many reasons. AAO membranes are thermally and chemically stable at high temperatures and in many environments. They are mechanically rigid, and can be easily dissolved in high or low pHs.

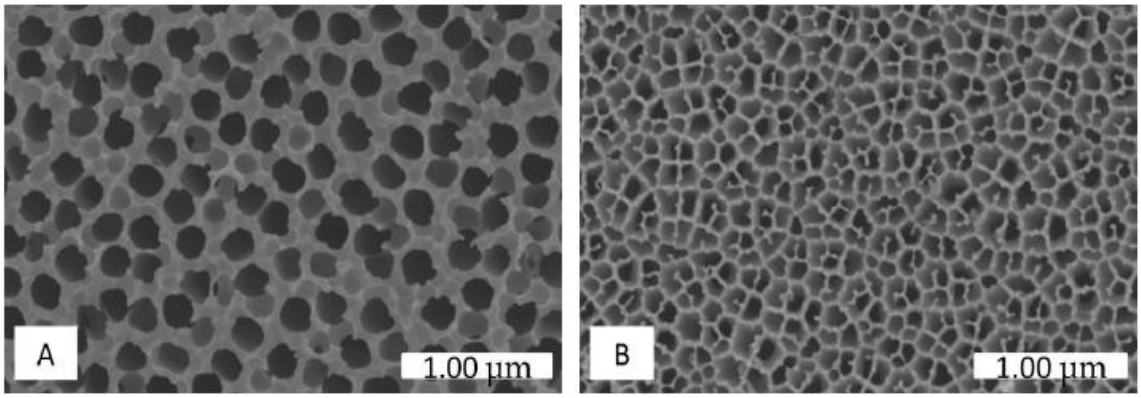

Figure 1-6. Electron micrographs of 200nm Whatman Anodisc^{TM} alumina template membrane. (A) Unbranched face with ~250 nm pores. (B) Branched face with 100-200 nm pores

The AAO membranes involved in this study were purchased commercially from Whatman Anodisc^{TM}. These membranes have an average thickness of 60µm and possess a very high pore density ($1.8x10^9$ pores/cm^2) of parallel, monodisperse, virtually cylindrical pores. Anodisc ^{TM} membranes are manufactured in 3 nominal pore size diameters: 0.02 µm, 0.1 µm, and 0.2 µm. The pores are called nominal because their diameters are actually much larger (200-250nm) through about ~98% of the membrane thickness and changes to a much smaller diameter for the last 2% of the

membrane thickness. The original large diameter pores branch into several smaller pores for the last 2% of the membrane thickness.

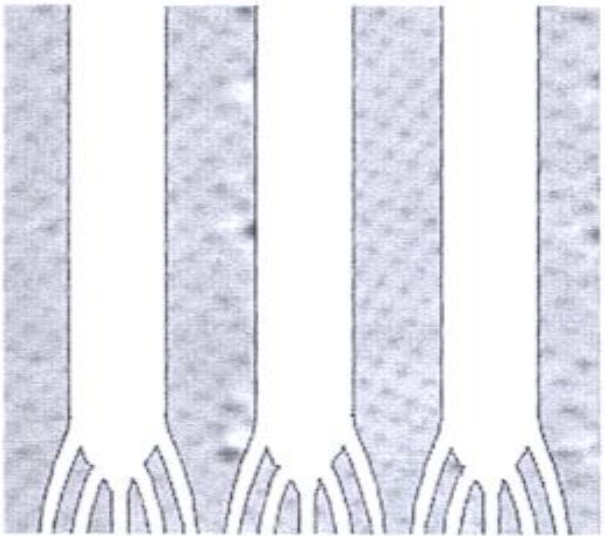

Figure 1-7. Illustration of anodic alumina membrane with branched pores

This branching is a result of the method by which the manufacturer fabricates these membranes. Aluminum oxide (alumina) is a product of the oxidation of aluminum foil in an acid at a particular voltage. The alumina grows as a porous honey-comb film attached to the aluminum foil. Once the alumina film has reached a desired thickness the oxidation is discontinued and the alumina is separated from the aluminum.

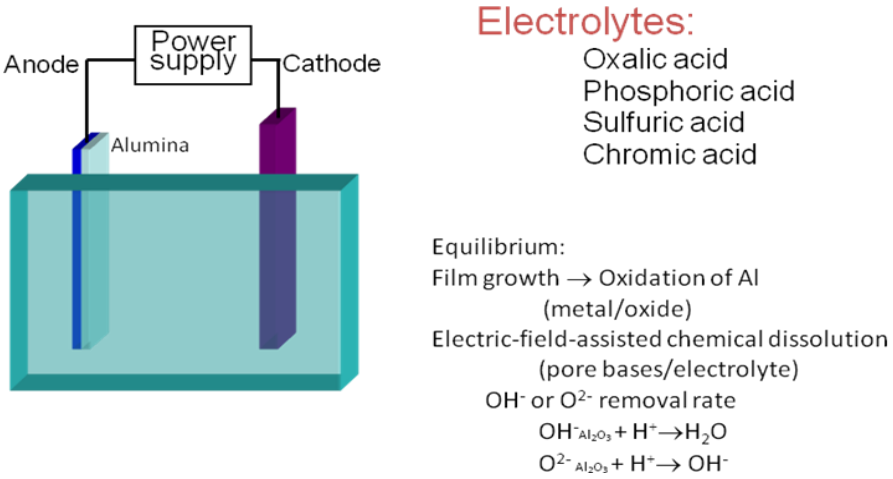

Figure 1-8. Alumina Fabrication

There are two methods generally used to separate porous alumina film from aluminum foil. These methods are chemical etching and voltage step reduction separation. In the chemical etching technique, anodization is discontinued once the porous film reaches the desired thickness. The aluminum template is then placed in a chemical solution where the aluminum and the alumina barrier layer is chemically etched away producing a free-standing porous alumina membrane. Alternatively, in voltage reduction separation, once the membrane has nearly reached the desired thickness the voltage is slowly reduced at periodic intervals. As the voltage is reduced the pores growing in the film branch off into smaller pores with thinner alumina walls. Anodization is discontinued once the alumina walls are thin enough to quickly dissolve in an acidic solution. The layer of the alumina with the narrowest walls will dissolve most quickly, leaving a free-standing defect free porous film separated from the aluminum foil.

The manufacturer uses the voltage step reduction separation method to fabricate the alumina membranes which explains the branched pores. In this study we chose to use Whatman Anodisc ^{TM} particularly because they are readily available in large quantities, inexpensive, easy to handle, and are of consistent quality.

Electrokinetics

Electrokinetics defines those processes where a charged fluid-solid interface reacts to external influences. Electrokinetics is often categorized into four distinct areas, as shown in Table (1-1).

Streaming potential and sedimentation potential are concerned with the generation of an electric field due to forced fluid or solid motions, where charged fluid-solid interfaces are present. These phenomena are not the focus of this research and the

interested reader should seek elsewhere for more in-depth treatment of these occurrences.[63-64] The remaining two electrokinetic phenomena, electroosmosis and electrophoresis, are of significance to the research herein but only electroosmosis will be discussed in detail.

Table 1-1. Classification of electrokinetic phenomena

Name	Movement Description	Action
Electroosmosis	Liquid moves relative to a stationary liquid	Applied electric used to induce movement
Electrophoresis	Charged surface moves relative to a stationary liquid	Applied electric used to induce movement
Streaming potential	Liquid moves relative to a stationary charged surface	Movement used to create an electric field
Sedimentation potential	Charged surface moves relative to a stationary liquid	Movement used to create an electric field

The idea of electroosmosis dates back to the research of F.F. Reuss who discovered the phenomena in 1809.[65] Electroosmotic flow operates by moving a liquid past a stationary surface by an electric field. To truly understand and appreciate the electroosmotic process we must discuss the electrical double layer.

Electrical Double Layer

When an aqueous medium comes into contact with solid surfaces, mechanisms such as ionization, ion adsorption and ion dissolution typically take place. These mechanisms result in the surface acquiring a charge. Depending on the polarity of the surface charge, a predominantly positive or negative charge near the surface will exist.

Ions of opposite charge to the wall, (counter-ions), are attracted to the surface of the wall and form a layer several Angstroms thick called the compact layer (also referred to as the Stern layer). These counter-ions in the compact layer are stationary and do not move relative to the surface. However, beyond the compact layer is another layer of ions, called the diffuse layer (also called the Gouy-Chapman layer). The diffuse

layer is comprised generally of counter-ions but co-ions (ions of the same charge as the wall) are also present in this region. The diffuse layer is thicker than that of the compact layer and the ions in the diffuse layer are mobile. In general the thickness of the diffuse layer will be approximately 3 to 5 times that of the compact layer. The imaginary interface between the compact and diffuse layer is called the shear plane.

The compact layer and the diffuse layer together are known as the electrical double layer (EDL) as shown in Figure 1-9.

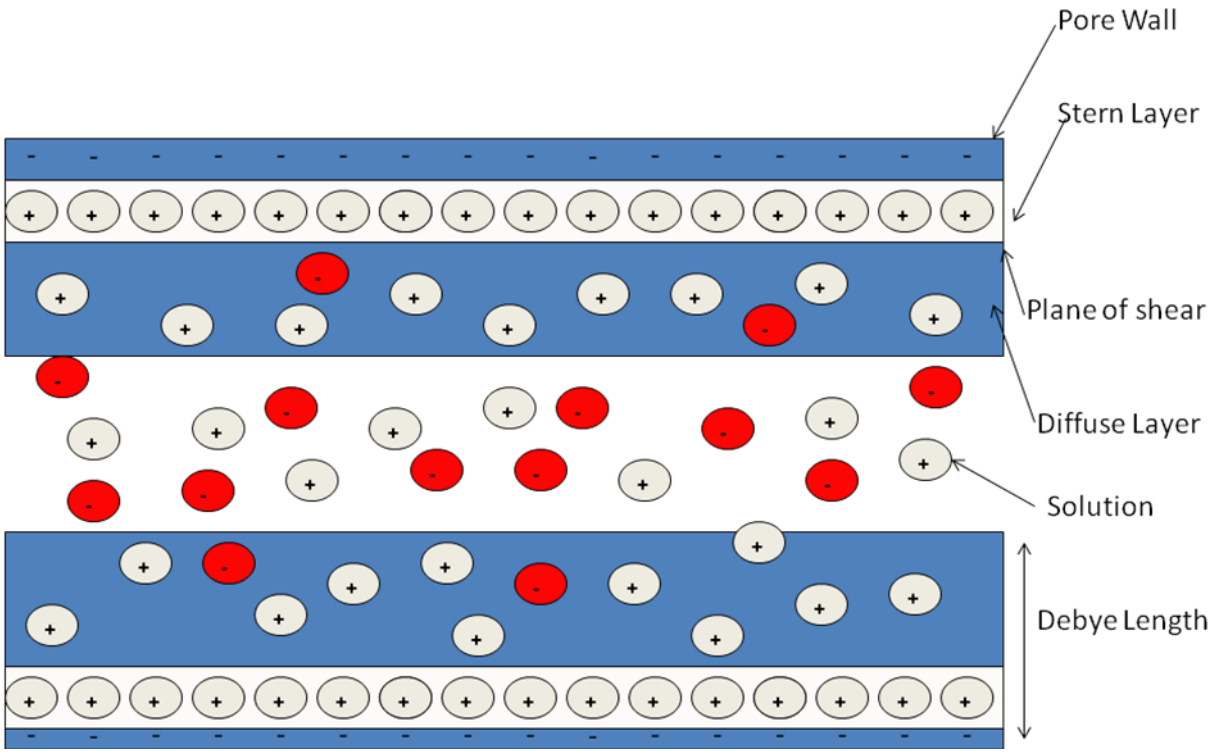

Figure 1-9. Illustration of the Electrical Double Layer

One of the major characteristics of the electrical double layer is the zeta potential (ζ). The zeta potential is the measure of the electrical potential at the plane of shear. It is characterized by Equation 1-1.

$$\zeta = \left(\frac{2kT}{ze}\right)\sinh^{-1}[(\sigma\kappa^{-1})]\frac{ze}{2\varepsilon kT} \qquad (1\text{-}1)$$

Where k is the Boltzmann constant, T is the temperature, z is the counter ion charge, e is the electrolyte charge, ε is the permittivity of water, κ^{-1} is the debye length and σ is the surface charge density at the plane of shear between the capillary wall and the electrolyte.

The zeta potential is used as a boundary condition for the potential at the point of zero velocity and is thus essential in calculations of electro-kinetic flows. Equation 1-1 simplifies to Equation 1-2 when solutions with relatively small zeta potentials are implemented.

$$\zeta = \sigma\kappa^{-1}/\varepsilon \tag{1-2}$$

When the electrolyte is symmetrical and is at 25°C, κ^{-1} is related to the concentration of the electrolyte by Equation 1-3 where z is the charge of the electrolyte and c the concentration of the electrolyte.

$$\kappa^{-1} = 9.61 \times 10^{-9}(z^2c)^{-1/2} \tag{1-3}$$

The last important feature of the EDL that will be discussed in this thesis is the length of the EDL, which is defined by the Debye length, or Debye shielding distance, denoted by λ_D. The Debye length is an estimate of the approximate thickness of the EDL. It is derived from the Poisson equation and is shown symbolically as Equation 1-4 where k_B is Boltzmann's constant, ε is the permittivity of the fluid, T is the absolute temperature of the fluid; e is the elementary charge and n is the ionic strength of the fluid.

$$\lambda_D = \sqrt{\frac{k_B \varepsilon T}{e^2 n}} \tag{1-4}$$

From Equations 1-1 though 1-4, we observe that the size of the electrical double layer increases as the ionic strength of the electrolyte decreases. We also recognize the

relationship between the zeta potential and the concentration of the electrolyte. Thus we can make the following conclusions: First, the electrical double layer becomes thicker in lower concentration electrolyte solutions; second, the zeta potential in an aqueous environment increases with increasing surface charge and decreasing electrolyte concentration. Thus the size of the electrical double layer is a very important parameter when determining the influence of electroosmotic flow in fluidic channels.

Electroosmotic Flow

When an electric field is applied across the length of a fluidic channel, the charged molecules of a fluid will experience an electrostatic force. In the bulk fluid where the concentration of counter-ions and co-ions are equal, there is no induced movement from the electric field. However, the mobile counter-ions in the diffuse layer experience that same electrostatic force which causes them to migrate toward the oppositely charged electrode. Due to viscous interaction, the mobile ions in the diffuse layer drag the fluid in the bulk layer. In this way a fluid flow is created which is called electroosmotic flow (EOF).

The velocity v_{eof} of the EOF is described by the Helmholtz-Smochulowski equation which is describe in Equation 1-5

$$v_{eof} = \varepsilon\zeta E(x)/\eta \tag{1-5}$$

where η is the viscosity, ζ the zeta potential, and E(x) is the electric field gradient along the channel and ε is the permittivity of electrolyte solution. The electroosmotic mobility μ_{eof} is given by the Equation 1-6.

$$\mu_{eof} = \varepsilon\zeta/\eta \tag{1-6}$$

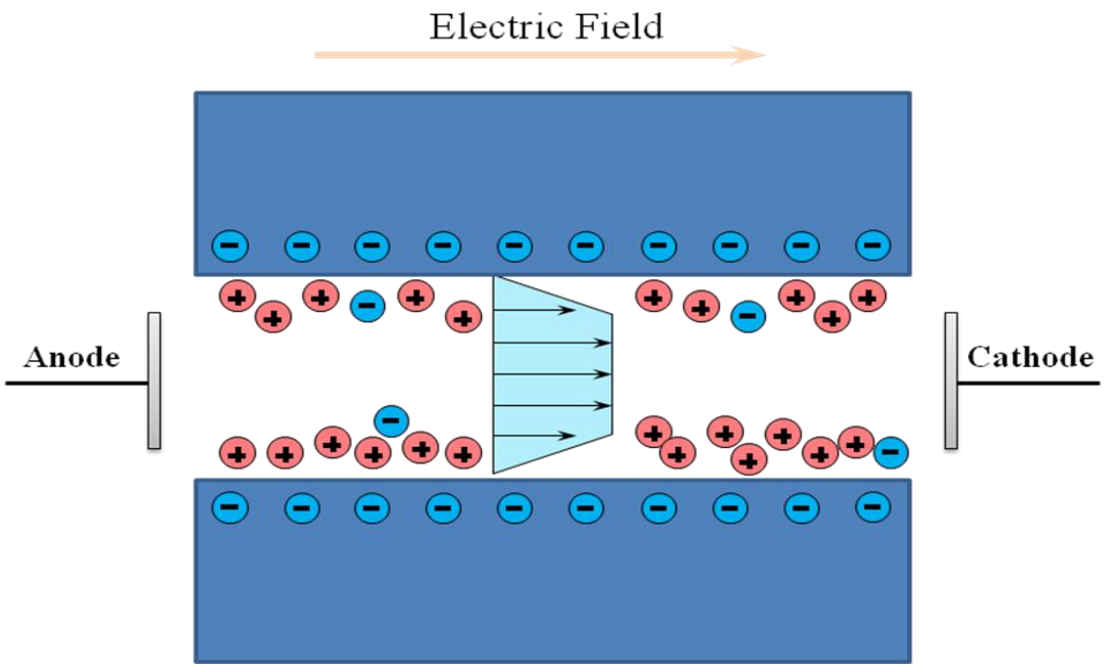

Figure 1-10. Schematic representation of electro osmotic flow

Thus, the electroosmotic volume flow q_{eof} through the channel is defined by Equation 1-7.

$$q_{eof} = \frac{\varepsilon \zeta}{\eta} \frac{A}{L} U \tag{1-7}$$

Here, A is the cross-sectional area of the channel, L its length, and U is the potential difference along the channel length.

Equations, 1-5, 1-6 and 1-7 show that the EOF is strongly dependent on the zeta potential. The zeta potential is not a constant; it is influenced by several factors which will be discussed in further detail in a later section of this thesis.

Electroosmotic flow versus pressure driven flow

To truly understand and appreciate the transport properties of EOF, there is a need to compare EOF to other flow transport mechanisms such as pressure-driven or hydraulic flow systems. One of the distinguishing characteristics among fluid flow systems are fluid flow profiles. Typically in EOF the fluid flow profile across the cross

section of a pore is flat or plug like. This is because the force that induces EOF originates in the diffuse layer of the EDL, which is very close to the pore wall. In contrast, in a pressure driven flow system the fluid flow profile is parabolic or laminar. The wall of the pore induces a frictional force upon the flow causing the velocity of the flow to be zero at the surface of the pore wall and to be slowed near the wall. The fluid velocity increases as the flow moves to the center of the fluidic channel and reaches it's maximum in the center of the pore, where fluid flow velocity is unhindered.

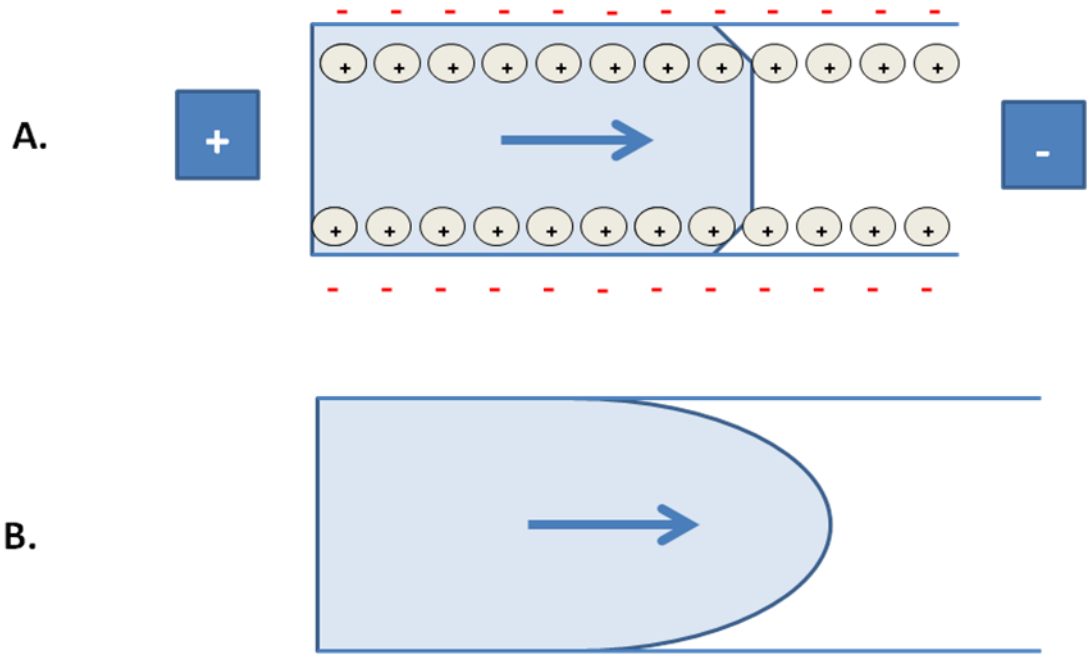

Figure 1-11. Comparison of fluid velocity profiles. A) EOF. B) Pressure driven flow

Another important characteristic that distinguishes EOF from pressure driven flow phenomenon is observed in the relative efficiency of each flow system as a function of pore radius. The hydraulic flow rate is proportional to $\pi a^4 v_{hy}$ (where a is the pore radius and v_{hy} is the flow velocity) while the electroosmotic flow rate is proportional to $\pi a^2 v_{eof}$. These equations imply that when the pore radius is large (>10cm) pressure driven flow

systems are most effective, but as the pore becomes smaller (on the order of the nano and micro scale) EOF becomes relatively more effective. [63]

In the Helmholtz-Smoluchowski equation (Equation 1-5) there is a limitation based on pore radius. In the Helmholtz-Smoluchowski equation, the assumption is made that most of the solution in a pore or capillary is always bulk solution, which is not always valid. When the diameter of a pore or capillary approaches the dimensions of the electrical double layer (i.e $\kappa^{-1}/z \approx 1$), the ideal environment of electroneutrality is lost. In this situation, the electrical double layer overlaps the pore diameter and the charged pore wall is no longer completely balanced by the counter- ions. Often in this case the pore will exhibit a certain level of permselectivity. Other conditions that make cause deviations from the Helmholtz-Smoluchowski theory are large zeta potentials, increases in surface conductance, changes in permittivity, and changes in viscosity within the pore or pores of interest. Another point of discussion is the case when $\kappa^{-1}/z \geq 1$. In this environment the driving force of EOF is extended throughout the entire pore cross section, the flow will experience a frictional force at the pore wall. As a consequence of this frictional force the flow velocity will be slow near the pore wall and the fluid flow velocity profile will be parabolic instead of plug-like. Thus the EOF will be will less effective, efficient, and more difficult to control in environments where $\kappa^{-1}/z \geq 1$.

Modulation of electroosmotic flow

As stated earlier, the zeta potential is an important parameter in EOF systems. From the Helmholtz-Smoluchowski equation we observe that EOF scales with the magnitude of this potential. Therefore it is important to be able to influence and control this potential. In general, for a solid surface the zeta potential is dependent on the bulk ionic concentration, valence of the ions, and pH of the solution (pH has the ability to

change the zeta potential from positive to negative). However, the zeta potential can also be altered by changing the microchannel surface material (e.g. from glass to PDMS) or by placing coatings on the microchannel wall.

In addition, the zeta potential is influenced by the ionic strength of the electrolyte solution since a higher ionic strength leads to a compression of the electric double layer. As a result of this compression the zeta potential will be reduced.

Other parameters that may influence the zeta potential are the chemical modification of the capillary wall, the addition of surface-active species or organic modifiers to the buffer, and the application of an external voltage to the system to regulate surface charge.

Thesis Overview

In Chapter 2, we describe the utilization of the template method to fabricate carbon nanotube membranes. This method entails synthesis of carbon nanotube membranes by chemical- vapor deposition within the pores of high pore density alumina membrane templates. We thoroughly explain the advantage of exploiting the flexibility in customizing nanostructures with specific characteristics by using the template method. We illustrate methods of controlling specific parameters of chemical vapor deposition which produce different properties in the carbon nanotube membrane. Lastly, we discuss the methods of characterization for the CNM.

In Chapter 3, we describe EOF in carbon nanotube array membranes. EOF was driven across the CNM by placing the membrane between two electrolyte solutions and placing an electrode in each solution to pass a constant current through the nanochannels of the membrane. EOF was monitored by measuring the flux of a probe molecule across the membrane. The CNMs have an anionic surface charge, which

results in EOF in the direction of cation migration across the membrane. EOF was used to control the flux of the probe molecule (phenol). When EOF was driven in the direction of diffusion there was an increase in the flux of the probe molecule across the membrane. Reversing EOF decreases flux in the direction of diffusion. At very high reversal EOF velocities, transport in the direction of diffusion becomes negligible and net transport proceeds in the opposite direction.

EOF through the CNM was modified by changing the pH, ionic strength and the current density applied to the membrane. These changes resulted in changes in the zeta potential. As stated earlier, the zeta potential is an important parameter in EOF systems. From the Helmholtz-Smoluchowski equation (Equation 1-5), we observe that EOF scales with the magnitude of this potential. Therefore it is important to be able to influence and control this potential.

CHAPTER 2
SYNTHESIS OF CARBON NANOTUBE MEMBRANES BY THE TEMPLATE METHOD

Introduction

Since their initial discovery in 1991 by Iijima[22-23], CNTs have generated much interest for their unique properties and possible applications. CNTs are a promising material for: field emitters [66], molecular electronics[67], strength enhancing filler materials[68], hydrogen storage [69-71] and molecular sieves [72]. New applications for CNTs are continuously being investigated and new discoveries are made every day.[73]

Recently, carbon nanotubes have been fabricated in arrays and utilized as membrane materials. As a membrane material carbon nanotubes are of significant interest due to the phenomenal properties that they possess. These properties include a high surface area, chemical and thermal stability, low production cost, and electrical conductivity.

When designing a membrane fabrication strategy there are several parameters to consider. These parameters include permeability, perm-selectivity, porosity, pore size distribution, material absorbance, and conformability. Many of these parameters are typically at odds with each other, thus it is important to have a fabrication strategy that can easily be customized for a given application.[74] There are many advanced membrane design strategies that have been employed to control pore length, diminish pore-size distributions, and maximize pore density. One such strategy is chemical vapor deposition of carbon onto the pore walls of a membrane. This method has been used to narrow and homogenize pore diameter and length.

Although considerable progress has been achieved by utilizing membrane design strategies, producing a mechanically strong membrane of defect-free, homogeneous,

aligned arrays of carbon nanotubes is still considered a daunting task. In the literature Sun and Crooks developed an inventive method of fabricating a CNM but with only a single multi-walled carbon nanotube. [75]

Alternatively, the Martin group and others have demonstrated the ability to grow CNM by CVD of carbon along the pore walls of nanoporous templates using a method called template synthesis (Figure 1-4) [48- 52]. Template synthesis offers the flexibility of using membranes on the order of 10^{11}nanopores per cm^2 [45-46]. The distinctive feature of template synthesis of CNTs by CVD is that the inner diameters of the CNT are tunable. Membranes have been prepared with nanotube diameters ranging from >100nm to <10nm.

Here, we discuss the advantages of template synthesis. We also illustrate the utility of this method by using it to fabricate CNMs. This is achieved by chemical vapor deposition of carbon into the nanopores of an anodic aluminum oxide membrane template.

The key advantage of template synthesis is the ability to customize nanostructures with specific characteristics. In this method nanotubes of carbon conform to the sizes and shapes of the respective host pores in which they are grown. Thus, there are a variety of design options available from which to choose.

By selecting specific design parameters we have extensive control of the carbon morphology and membrane characteristics. The carbon layer growth was controlled as a function of the CVD rate and time. At low CVD rates, carbon deposition is homogeneous and easily controlled as a function of time. However, at high CVD rates

carbon deposition becomes diffusion-limited and preferentially deposits at the mouths of the pores.

Experimental

Materials

Two types of Whatman Anodisc^{TM} Filter Membranes were used in diameters of 20nm or 200nm as templates. Ethylene (30% in helium) and argon were used as received. All other chemicals were reagent grade and used as received from Fisher Scientific (Fairlawn, NJ). All solutions were prepared using water that was purified by passing house-distilled water through a Barnstead (Dubuque, IA) E-pure water purification system. The carbon nanotubes discussed in this work were prepared in 200-nm templates unless otherwise stated.

Preparation of Carbon Nanotubes

The preparation of carbon nanotubes by template synthesis has been previously reported. [48, 50-51] The first step in CNM fabrication is heat pretreatment. Prior to CVD synthesis, the alumina template membranes were pressed between two quartz plates and heated to a temperature slightly above the CVD temperature for 1 hour in air. If this heat pretreatment is not done, the alumina membranes curl into a tight cylinder during the CVD synthesis of the carbon nanotube membrane. Heat pretreatment between the quartz plates prevent this unwanted curling, and allow for synthesis of planar carbon nanotube membranes.

After heat pretreatment a (2.2 cm x 1.5cm) piece of the heat treated alumina template membrane was placed vertically in the CVD reactor. The CVD reactor consisted of a quartz tube (diameter = 4.2 cm, length= 52 cm) that was placed within a tube furnace. The reactor temperature was increased to the designated deposition

temperature (650 °C-770°C), under constant argon flow. When the temperature stabilized, the argon flow was terminated, and simultaneously a 20-sccm flow of ethylene gas mixture was initiated.

Under these conditions ethylene pyrolyzes to yield carbon nanotubes within the pores of the template as well as a thin carbon film on both faces of the membrane. Deposition was continued for a prescribed amount of time. After the deposition the ethylene flow was terminated, the argon flow was resumed, and the furnace was turned off and allowed to cool to room temperature. After synthesis the membranes were stored in air for at least 24 hours prior to use.

The CVD temperature and time were varied for several reasons. The CVD temperature controls CVD kinetics and determines many of the properties of the carbon. The deposition time regulates the thickness of the carbon nanotube wall and surface layer of carbon on the membrane.

Characterization of Carbon Nanotube Membranes

X- Ray Photoelectric Spectroscopy

X-ray Photoelectric Spectroscopy (XPS) studies of the samples were performed on a Perkin Elmer 5100 XPS system spectrometer with Al Kα excitation (200 W) source. The samples were mounted onto a stainless steel sample stub by means of a 7 mm diameter carbon sheet disk (SPI Supplies), so as to completely cover both the carbon disk and the sample stub. The samples were inserted into the sample analyzer chamber by means of a quick insertion probe, and spectral acquisition with the fixed analyzer transmission mode commenced after the pressure decreased to 5 $x10^{-9}$ Torr. Survey scans, high-resolution C 1s spectra, and high resolution O 1s spectra were recorded at a takeoff angle of 20° relative to the sample surface. The information depth is estimated

to be 2.5 nm for C 1s. Data analysis was done by using the AugerScan software package. Peak positions were all referenced to 285.0 eV for the main carbon peak.

Electron microscopy

Transmission electron microscopy (TEM) and scanning electron microscopy (SEM) were used to visualize the carbon nanotubes prepared within the pores of the alumina template membrane. The carbon nanotubes were imaged both as a cross-section while still inside the alumina membrane and also as liberated individual nanotubes. This was achieved by first dissolving the alumina in a solution of 10% H_3PO_4 for 16 hours. The H_3PO_4 was removed by pipette leaving the liberated nanotubes, still connected together by the carbon surface films. The nanotube array was carefully rinsed with methanol and then suspended in methanol. This suspension was then ultra-sonicated for 20 minutes, which produced individual carbon nanotubes separated from the carbon surface film.

For the preparation of TEM samples a drop of the sonicated membrane suspension was applied to a Formvar Layered Carbon Type A TEM grid. The carbon nanotubes adhered well to the grid and were easily visualized with use of a Hitachi H-7000 transmission electron microscope.

For SEM imaging a drop of the suspension was applied to a piece of copper tape attached to a SEM stub. The solvent of the suspension was allowed to dry and gold was sputtered onto the sample to improve electrical conductivity. The images were acquired using a Hitachi S-4000 field emission scanning electron microscope.

Sheet resistance

Sheet resistance is a measurement of the resistance for thin films that are uniform in thickness. The sheet resistance was measured for the CNMs using a Lucas

Signatone SP4 4-point probe and a Keithley 2100 multimeter. The basic model for these measurements is illustrated in Figure 2-1.

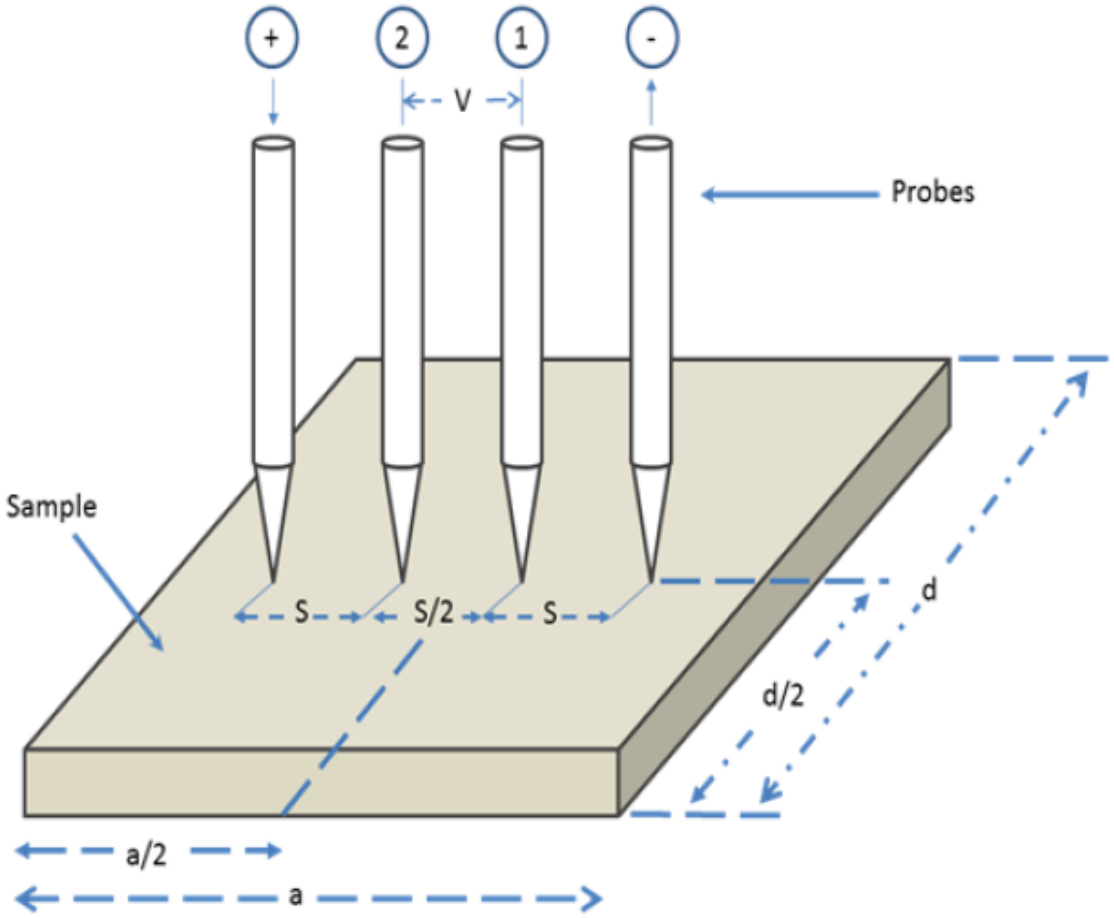

Figure 2-1. Basic setup for sheet resistance measurements

The sample is placed on a flat surface and four sharp probes make contact with the material to be measured. A constant input current is passed through the two outer electrodes, and the changes in voltages are measured across the inner pair of electrodes.[76-77]

The spacing of the probes plays key role in the sheet resistance measurement. If the spacing between the probe points is constant, and the conducting film thickness is less than 40% of the spacing, and the edges of the film are more than four times the

spacing distance from the measurement point, the average resistance of the film or the sheet resistance is given by Equation 2-1.[76-77]

$$\rho_s = 4.53\ x\ V/I \quad (2\text{-}1)$$

The thickness of the film (cm) and its resistivity (ρ cm) are related to ρ_s by Equation 2-2.

$$\rho s = \text{resistivity } (\rho \text{ cm})/\ \text{thickness(cm)} \quad (2\text{-}2)$$

Results and Discussion

As discussed previously, the Anodisc™ aluminum oxide membrane has an unbranched face and a branched face (Figure 1-5). At the branched face of the template the pore openings are irregularly shaped with diameters from 100~200 nm (Figure1-5). At the unbranched face of the template, the pore openings are circular with an average approximate pore diameter of 250 nm.

Each of the pores in the membrane serve as a cast for which the carbon nanotubes are grown. Thin layers of carbon film are deposited by CVD onto the pore walls of the membranes which create nanotubes. As stated earlier the morphology and dimensions of each nanotube is determined by the profile of the host pore in which it is grown.

Figure 2-2 displays a cross section of the carbon nanotube membrane. We measure the pore diameter and calculate the pore density from these electron micrographs. Figure 2-3 shows a TEM image of individual carbon nanotubes that have been detached from the carbon surface film after alumina dissolution following ultrasonication of the nanotube suspension. These images illustrate the consistency of the wall thickness throughout the entire length of nanotube. From these images a consistent wall thickness is obtained.

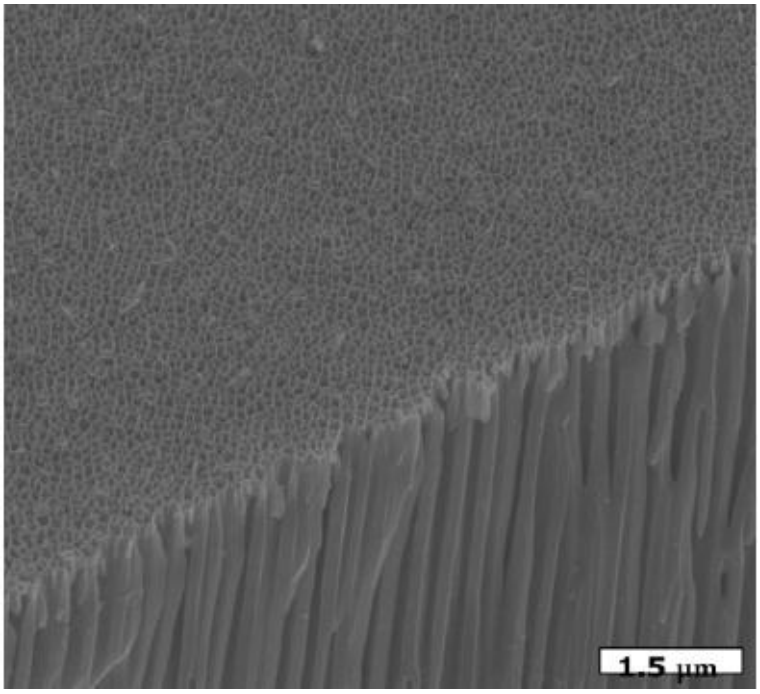

Figure 2-2. Electron micrograph of the cross section of carbon nanotube membrane

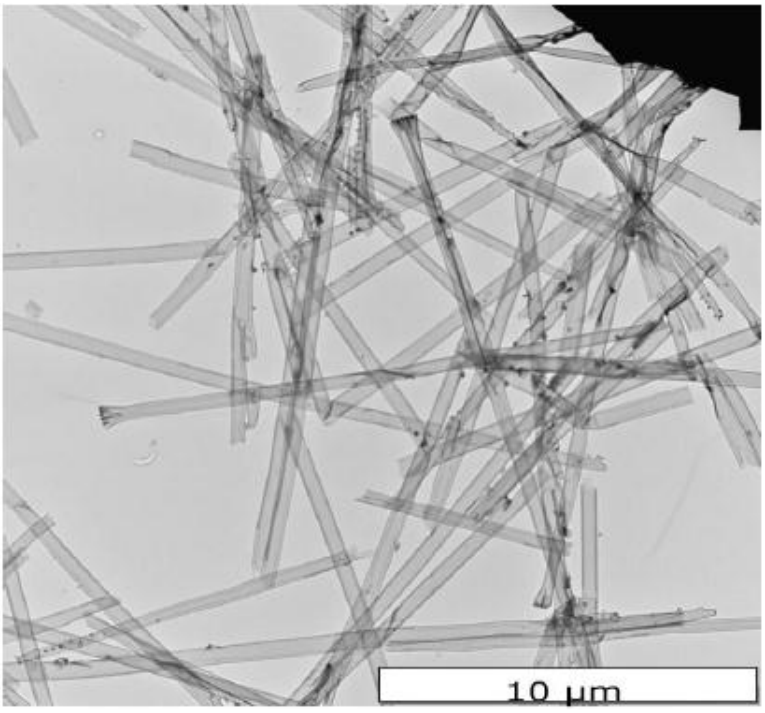

Figure 2-3. Electron micrograph of individual carbon nanotubes

Effect of CVD Rate on Carbon Nanotube Growth

Exercising precise control of the CVD rate of carbon nanotube growth inside the pores of the alumina membrane is of utmost importance. There are several factors that

affect the CVD rate including the diameter of the host pores, the deposition temperature and the gas flow rate. In this section we will very briefly discuss these parameters.

Chemical vapor deposition of carbon in a nanoporous alumina membrane is gas diffusion limited; as the pores of the nanotubes become narrower, the gas is more impeded and has a harder time passing through the whole length of the pore. As a result of this hindrance the CVD rate decreases.

We define the ratio of the mass of carbon to the mass of the alumina membrane (AAO) as % carbon in Equation 2-3.

$$\%\ \text{carbon} = \frac{(m_{fin} - m_{int})}{m_{int}} \times 100\% \qquad (2\text{-}3)$$

Here, m_{int} is the mass of the alumina template before carbon deposition and m_{fin} is the mass of the membrane after carbon nanotube growth.

The CVD rate is defined as the amount of carbon deposited onto a substrate per unit time of deposition at a constant temperature. Figure 2-4 displays a plot of percent carbon versus time of carbon deposition grown at 725^{o}C.

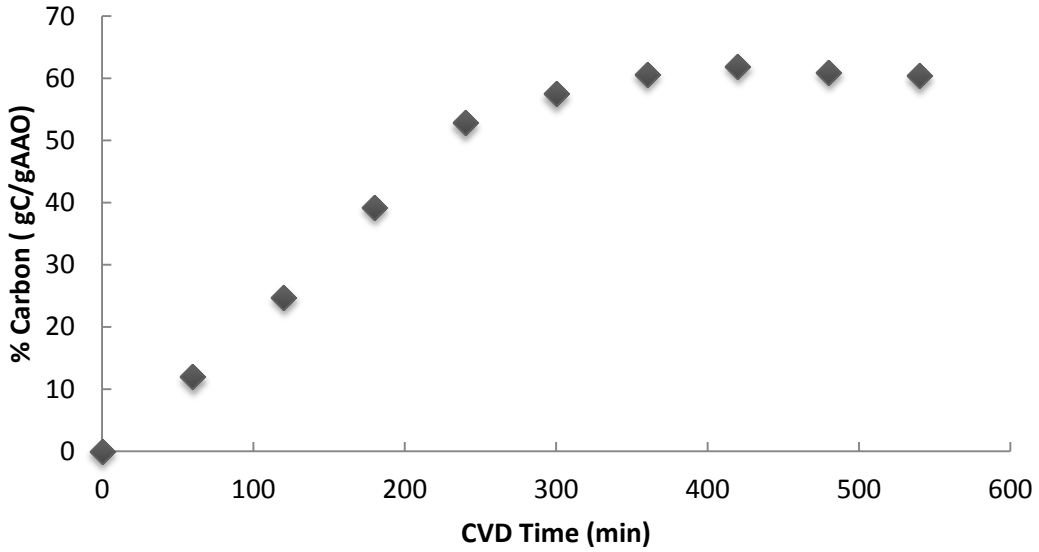

Figure 2-4. Plot of % carbon on the alumina template vs.CVD time

Initially there seems to be an approximant linear relationship between the percent carbon and the CVD time (CVD_T) but as the CVD_T is extended the percent carbon plateaus. This can be explained by investigating the relationship between the mass of the carbon deposited and the surface area of the substrate. According to the literature,[78] the pore walls of the 200-nm Anodisc™ membrane comprise more than 99%of the total surface area of these membranes. As the carbon is deposited onto the pore walls of the membrane the diameter of the pores becomes narrower, which produces a significant drop in surface area of the membrane. As seen in the plot, it is hypothesized that at some point in the deposition the carbon has essentially closed the pore, which means deposition would only continue on the template surface and not inside the pore.

From the slope of the plot displayed in Figure 2-4, the CVD rate can be predicted for short duration depositions at a given temperature. An average CVD rate can be calculated from Equation 2-4.

$$R_{CVD} = \frac{(m_{fin} - m_{int})}{m_{int} \times t_{CVD}} \quad (2\text{-}4)$$

Effect of Temperature on CVD Rate

It has been concluded that at high temperatures CVD reactions occur more rapidly.[79] When the temperature is very high (>850) the vapor deposition reactions occur so rapidly, that the carbon deposition is non-uniform along the length of the nanotube. Diffusion is considered to be a slow process, when the temperature is high the CVD reactions occur so fast that diffusion can no longer maintain equilibrium throughout the thickness of the membrane; thus a carbon concentration gradient develops along the length of the nanopore. In Figure 2-5, we display that as the temperature increases the average CVD rate also increases. When a low CVD temperature (<750) is selected the

result is usually a CNM with uniform wall thickness. The duration of low temperature CVD typically results in thicker or thinner nanotube walls. This utility allows for the customization of the CNMs with a variety of pore diameters.

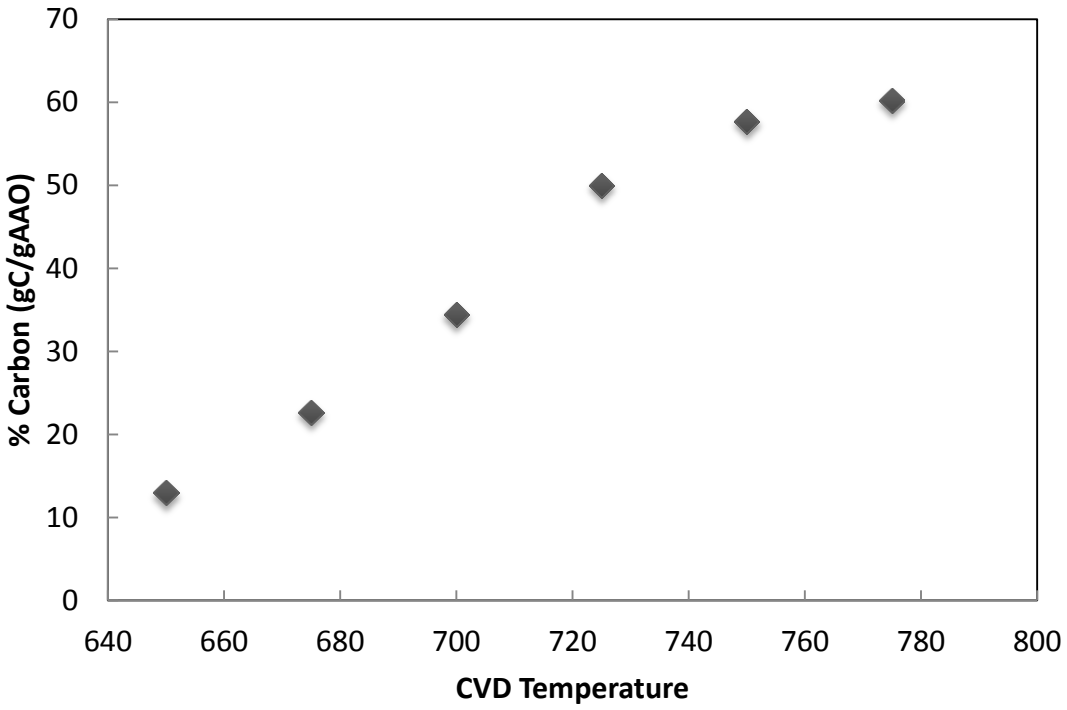

Figure 2-5. Plot of % carbon vs. CVD temperature

Conclusion

Carbon nanotubes are of great interest in both fundamental and applied science. Our group has created template-synthesized carbon nanotubes by chemical vapor deposition of ethylene gas onto commercial alumina membranes. By utilizing this method carbon nanotubes can be grown with tailored properties, dimensions, and shapes. The key feature of template synthesis is that each carbon nanotube conforms to the pore morphology of the template membrane. Each nanotube has an inner diameter defined by the thickness of the tube wall and the diameter of the host pore.

The CNMs prepared in the alumina templates contain parallel, homogeneous, dense, arrays of aligned monodisperse carbon nanotubes.

We have employed a number of design strategies to modify and control carbon nanotube growth inside the alumina membrane. Controlling the CDV rate by modifying certain CVD conditions have been investigated. From the results we conclude that conducting CVD at a low temperature (<770^{o}C) and for durations less than 7 hours will produce the most consistent and reproducible CNM.

The carbon nanotube membranes (CNM) discussed in this work are used for fundamental electrochemical investigations. They are used specifically as tools to monitor and control electroosmotic flow (EOF).[10,43] Although nanotubes grown in the 200-nm Anodisc^{TM} templates are not exactly perfect cylinders, they are inexpensive, commercially available and of consistent quality. They are ideal for electroosmotic flow permeation experiments and have been used in past research endeavors.[50,62]

CHAPTER 3
ELECTROOSMOTIC FLOW IN CARBON NANOTUBE MEMBRANES PREPARED BY THE TEMPLATE SYNTHESIS METHOD

Introduction

Carbon nanotubes (CNTs) have attracted great interest due to their remarkable electronic, optical, and mechanical properties. Potential applications for carbon nanotubes range from fundamental research, to the development of new devices. The Martin group and others have created template-synthesized carbon nanotubes by chemical vapor deposition of ethylene gas onto commercial alumina membranes. By utilizing this method carbon nanotubes can be grown with tailored properties, dimensions, and shapes. The key feature of template synthesis is that each carbon nanotube conforms to the pore morphology of the template membrane. Each nanotube has an inner diameter defined by the thickness of the tube wall and the diameter of the host pore. The CNMs prepared in the alumina templates contain parallel dense arrays of aligned monodisperse carbon nanotubes.

It has recently been suggested that carbon nanotube membranes could possibly be used as separator membranes in Li-ion batteries. A battery separator is a porous membrane placed between the anode and cathode of a battery. The main function of a separator is to keep the positive and negative electrodes apart in order to prevent electrical short circuits, while also allowing the transport of ionic charge carriers.[80]

Relative to the amount of research on electrode materials and electrolytes, very little attention has been aimed at characterizing and developing new separator materials. The most important requirements for Li-ion battery separators are permeability, porosity, chemical and thermal stability, pore size, and electrical

resistance. Many of these characteristics are available and tunable in template prepared CNMs.

The research results presented in this thesis have been aimed at studying the fundamental transport processes occurring at the interface of a porous carbon nanotube membrane and an electrolyte by monitoring and controlling electroosmotic flow (EOF). EOF refers to the movement of solution past a stationary surface due to an externally applied electric field. Building upon previous investigations, [50, 62] we demonstrate here, the effects of pH, ionic strength, and applied transmembrane current on the EOF by monitoring and measuring the flux of a probe molecule across the cylindrical pores of carbon nanotube membranes [50, 62, 81-83]. The as-synthesized CNMs have anionic surface charge, and as a result, EOF is in the direction of cation migration across the membrane. The results from this research should provide some of the fundamental information needed to understand a practical approach for using a carbon nanotube membrane as a possible new material for advance battery separators.

Experimental

Materials

Whatman Anodisc™ Filter Membranes with 200-nm pores were used as template membranes. Ethylene (30% in helium) and argon were used as received. Buffer solutions were prepared from monobasic sodium phosphate and the pH was adjusted with 1 M NaOH and 1 M HCl. Phenol was obtained from Sigma-Aldrich (St. Louis, MO). All other chemicals were reagent grade and used as received from Fisher Scientific (Fairlawn, NJ). All solutions were prepared using water that was purified by passing house-distilled water through a Barnstead (Dubuque, IA) E-pure water purification system.

Preparation of CNM

The CVD method used to prepare these carbon nanotubes has been described previously in Chapter 2 of this thesis and elsewhere in the literature [48, 50-51]. Briefly, the alumina template membrane was pressed between two quartz plates and heated to 750^{o} C for 1 hour in air prior to chemical vapor deposition. This heat pretreatment is done to prevent unwanted curling of the alumina membrane during the CVD synthesis of the carbon nanotubes. After heat pretreatment a (2.2 cm x 1.5cm) piece of the alumina template membrane was placed vertically in the CVD reactor in the tube furnace. The reactor temperature was increased to 725°C, under argon flow. When the temperature stabilized, the argon flow was terminated, and simultaneously a 20-sccm flow of an ethylene gas mixture was initiated for 4 ½ hours. After deposition the argon flow was resumed, and the ethylene flow was terminated. After carbon nanotube synthesis the membrane was stored in air for at least 24 hours. CNMs prepared in this way are classified as "as-synthesized" membranes and have an anionic surface charge.

EOF Measurements

The permeation measurements in this study were conducted with a CNM assembly. The CNM assembly as shown in Figure 3-1 is a modified assembly that was originally fabricated by Miller et al.[90, 88 50, 62]. The assembly is composed of two acrylic slides, two pieces of parafilm, two parafilm washers, the carbon nanotube membrane and a piece of conductive copper tape attached to the membrane. The various components of the assembly were secured by heating the membrane assembly in an oven at 125°C for 5 min. The heat caused the parafilm to melt, which acted as a glue to hold the various pieces together.

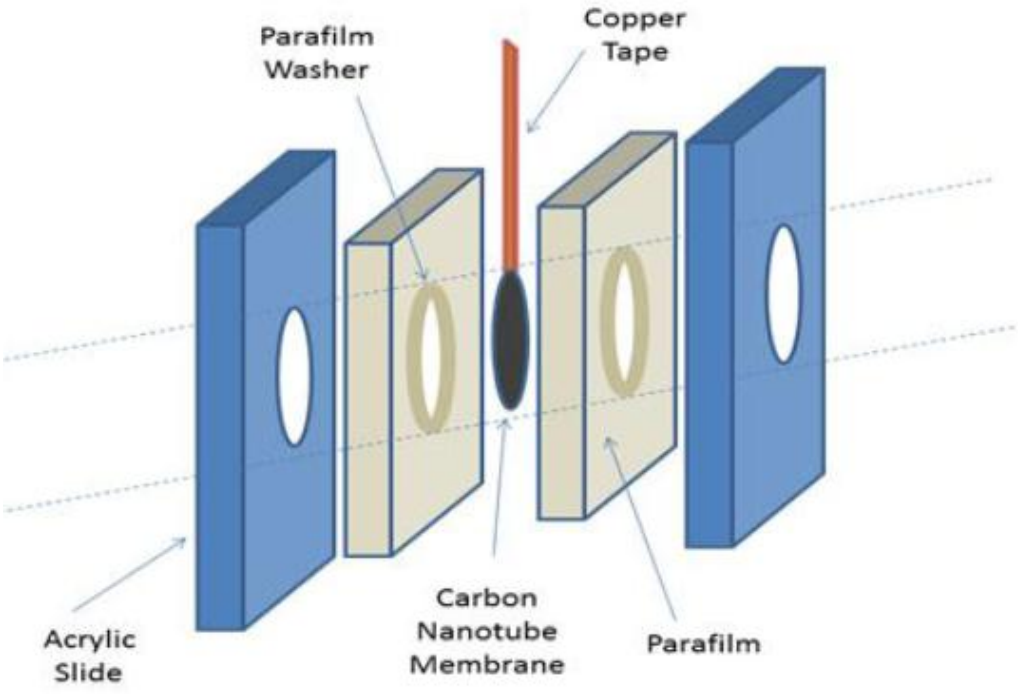

Figure 3-1. Illustration of the carbon nanotube membrane assembly

Electroosmotic flow (EOF) measurements were made in simple U-tube permeation cells.[50,62, 83] This assembly exposed a 0.495 cm^2 area of the CNM to the electrolyte solution. As with previous reports,[50,62, 81-83] the rate of EOF was determined by measuring the flux of a neutral probe molecule across the membrane or in this case the membrane assembly. The carbon nanotube membrane assembly was clamped between the two halves of a U-tube cell. The membrane assembly was exposed to the electrolyte solution on one side (permeate side) and electrolyte solution with 10 mM phenol added to it on the other side (feed side).

A platinum wire electrode was placed in each solution, and a constant transmembrane current was supplied using an EG&G 263A galvanostat. As stated in the previous section, the as-synthesized membranes have an anionic surface charge, which means the direction of EOF will initially be toward the cathode. The galvanostat was configured as illustrated in Figure 3-2, such that the reference/counter electrode

(cathode) was positioned on the permeate side and the working electrode (anode) was located in the feed side.

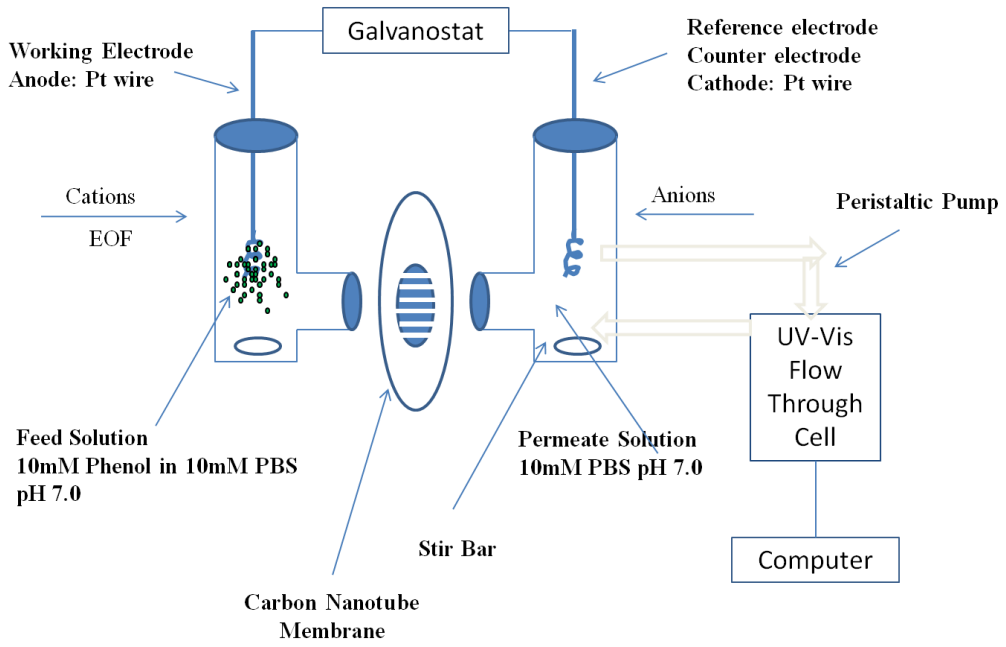

Figure 3-2. Schematic of permeation cell used in EOF experiments

Results and Discussion

Effect of Applied Current Density on Permeate Flux

The flux of the probe molecule is directed related to the magnitude and direction of the current. Figure 3-5 shows a plot of micromoles of phenol transported across the carbon nanotube membrane as a function of applied current density. This plot consists of five linear curves, and the slope of each curve is the flux of phenol (N_J) at that applied current density as seen in Table 3-1.

The dark blue linear curve in Figure 3-1 was diffusive flux (N_{diff}), which means these measurements were obtained with no applied current. The flux in this case is only from the diffusion of phenol molecules from the feed side across the membrane and into the permeate half cell. The purple linear curve was obtained with an applied current

density of J_{app}= -6.06 mA/ cm^2. The flux of phenol across the membrane in this linear curve was observed to decrease below that of the diffusion curve indicating that EOF is in the opposite direction of the diffusive flux (EOF from permeate solution to feed solution).

This concept is confirmed by data in the red linear curve, which were obtained with J_{app} = +6.06 mA/ cm^2. This data display a net flux that is higher than the diffusive flux, which signifies EOF in the direction of diffusive transport. The concluding two linear curves were obtained at higher positive and negative applied current densities and further enhancement and diminution in the flux were respectively observed as a result.

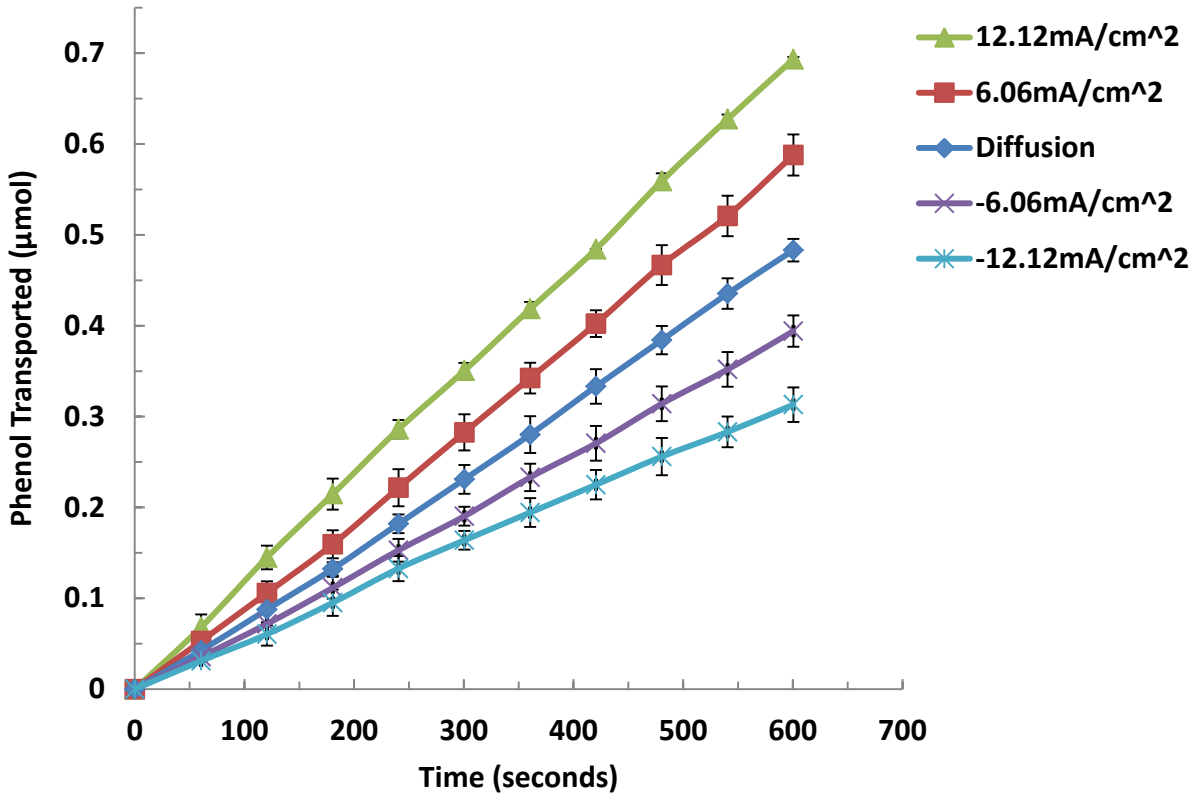

Figure 3-3. Plot of phenol transport vs. time at different current densities

Table 3-1. Effect of applied current density on the flux, enhancement factor, peclet number and the electroosmotic flow velocity of phenol through the carbon nanotube membrane.

J_{app} mA/cm^2	Flux nmol/(s*cm^2)	E N_J/N_{Diff}	Peclet Number	v_{eof}, µm/s
-12.12	0.53	0.65	-.081	-13.07
-6.06	0.67	0.83	-0.36	-5.81
0.00	0.81	1.00	0.00	0.00
6.06	0.98	1.21	0.39	6.29
12.12	1.21	1.49	0.86	13.87

***** The geometric area of the membrane was 0.495 cm^2

Calculation of the Electroosmotic Velocity

The Nernst-Plank equation was used to describe the steady-state flux of permeante molecules across a membrane in the presence of an applied transmembrane current.

$$N_J = -D[\partial C(x)\partial x] - zF/(RT)DC[\partial\phi(x)\partial x] \pm Cv_{eof} \quad (3\text{-}1)$$

In Equation (3-1), D is the diffusion coefficient, C is the concentration, and z is the charge of the permeate molecule, respectively. ∂C(x)/δx is the concentration gradient in the x direction across the membrane, $\partial\phi(x)\partial x$ is the potential gradient of the electrolyte within the nanotubes, and v_{eof} is the electroosmotic velocity. The Nernst-Plank equation separates molecule transport into three distinct terms that describe the diffusive, migrational, and EOF convective transport processes. Since phenol is a neutral molecule at the pH used in these experiments Equation 3-1 simplifies to Equation 3-2.

$$N_J = -D[\,\partial C(x)\partial x]\,] \pm Cv_{eof} \quad (3\text{-}2)$$

When there is no applied current (J_{app}= 0), the flux is only generated by diffusion, so only the first term in Equation 3-2 becomes operative (N_{diff}). A parameter called the enhancement factor, *E* can be calculated from the experimental flux data in Table 3- 1.

The enhancement factor can then be used to calculate the electroosmotic velocity as seen in Equation 3-3.[82]

$$E = N_J / N_{diff} \quad (3\text{-}3)$$

E is the ratio of the flux in the presence of an applied current, to the diffusive flux (flux at $J_{app} = 0$). The enhancement factor (*E)* values for the data in Figure 3-5 are shown in Table 3-1. *E* is greater than unity when a positive current is applied. This result indicates that EOF is in the direction of the diffusive flux. Analogous results were obtained by Miller et al. for carbon nanotube membranes, where EOF is due to the membranes fixed carboxylate sites.[83] From these results, we confirm that for air-treated carbon, the pore walls on the carbon nanotubes have fixed negatively charged sites.[85-87]

The peclet number is the ratio of pure EOF flux to diffusive flux. It can be calculated from the equation Srinivasan and Higuchi applied to demonstrate the relationship between the enhancement fact (E) and peclet number (Pe). [84]

$$E = Pe \,/\, ((1 - (\exp(-Pe))) \quad (3\text{-}4)$$

The peclet number can then be used to calculate v_{eof} using Equation 3-5.

$$v_{eof} = Pe \times (\frac{D}{l}) \quad (3\text{-}5)$$

In Equation 3-5, l is the thickness of the membrane, and D is the bulk solution diffusion coefficient. From Table 3-1, we observed that current densities of the same magnitude but opposite sign give EOF velocity values of approximately the same value but opposite signs.

The Helmholtz-Smoluchowski equation[63] depicts the relationship between the electroosmotic velocity and the linear electric field gradient ($E(x)$, V cm^{-1}) across the membrane.

$$v_{eof} = -\varepsilon\zeta E(x)/\eta \quad (3\text{-}6)$$

In Equation 3-6, ε is the permittivity of water, ζ is the zeta potential, E(x) is the electrical field gradient (E/l), and η is the viscosity of the solution. If we substitute the product of the applied current density and the resistivity of the electrolyte within the nanotubes ρ, for E(x) in Equation 3-6 we derive Equation 3-7.

$$v_{eof} = -\frac{\varepsilon\zeta J_{app}\rho}{\eta} \quad (3\text{-}7)$$

Equation 3-7 reveals the linear relationship between the applied current density and the v_{eof}. From the Figure 3-3, we observe that the flux increases with increasing positive applied current density (J_{app}). This result indicates that EOF plays a substantial role in the transport of permeate across the membrane. At sufficiently negative J_{app} values, the net flux approaches zero. In this case, EOF from the permeate half-cell to the feed half cell is canceling out the diffusive flux from feed to permeate.[81]

Effect of ionic strength of electrolyte on v_{eof}

Data was collected from the transport of phenol at a constant applied current density of 10 mA/cm^2 and at a various ionic strengths. As seen in Figure 3-4 the ionic strength ranged from 0.01M to 0.60M. The pH of the electrolyte was maintained at 7. The general tread of the plot shows that as the ionic strength increases the v_{eof} decreases as is expected.

We observe from Equation 3-7 that veof is directly related to the zeta potential. The zeta potential is related to the Debye length $k^{-1}$by Equation (3-8)[88].

$$\zeta = \left(\frac{2kT}{ze}\right)\sinh^{-1}(\sigma\kappa^{-1}\, ze/(2\varepsilon kT)) \quad (3\text{-}8)$$

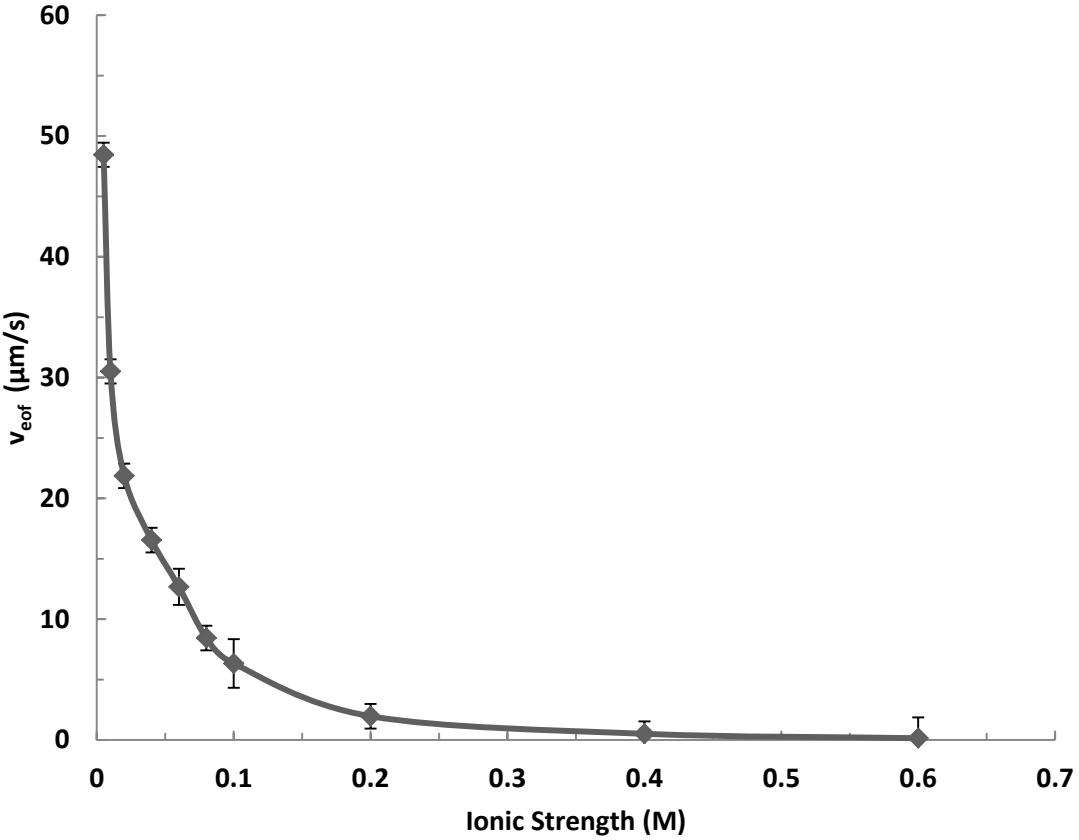

Figure 3-4. Plot of electroosmotic flow velocity vs. ionic strength of permeate and feed solutions. Applied current density was +10 mA/ cm^2.

Here, k is the Boltzmann constant, T is the temperature, z is the counter ion charge, e is the electrolyte charge, ε is the permittivity of water, κ-1 is the Debye length and σ is the surface charge density at the plane of shear between the capillary wall and the electrolyte. The zeta potential is used as a boundary condition for the potential at the point of zero velocity and is thus essential in calculations of electrokinetic flows.

When solutions with relatively small zeta potentials are utilized in permeate experiments Equation 3-8 simplifies to Equation 3-9.

$$\zeta = \frac{\sigma\kappa^{-1}}{\varepsilon} \tag{3-9}$$

When the electrolyte solution is symmetrical and is at 25^{o}C, κ^{-1} is related to the concentration of the electrolyte by Equation 3-10.[63]

$$\kappa^{-1} = 9.61 \times 10^{-9}(z^2 c)^{-\frac{1}{2}} \quad (3\text{-}10)$$

In Equation 3-10, z is the charge of the electrolyte and c is the concentration of the electrolyte. From this equation we observe that the double layer thickness decreases with increasing ionic strength of the electrolyte, which means that the ζ-potential decreases with increasing ionic strength (Equation 3-9).This information explains one of the reasons why v_{eof} decreases with increasing ionic strength, which is experimentally observed in Figure 3-4.

From Equation 3-7 we observe that another factor contributes to the observed decrease in v_{eof} with increasing ionic strength. The resistivity of the electrolyte ρ, is also proportional to the v_{eof}. The resistivity is inversely proportional to the number of charge-carrying ions in the solution. Therefore, ρ decreases with increasing ionic strength of the electrolyte, and Equation 3- 7 indicates that this would also contribute to the observed decrease in v_{eof} with increasing ionic strength as observed in Figure 3-4. For these reasons we observe that when the highest ionic strength electrolytes are employed the electroosmotic velocities decrease close to zero.

Effect of solution pH on v_{eof}

The v_{eof} versus solution pH data are shown in Figure 3-5. The transport of phenol was monitored at applied current densities of positive 15 mA cm^{-2} in electrolyte solutions that were 10 mM in NaCl and 0.5 mM in phosphate buffer, and with the pH adjusted to values between 3 and 7. The NaCl served to maintain the ionic strength at a constant value.

The plot followed an expected trend considering EOF is a charge dependent phenomenon and the surfaces of the CNMs have anionic surface charge. At high pH values where the negative surface charge is enhanced, the v_{eof} is also enhanced. Alternatively at low pH values where the negative surface charge is diminished, the v_{eof} is also diminished.

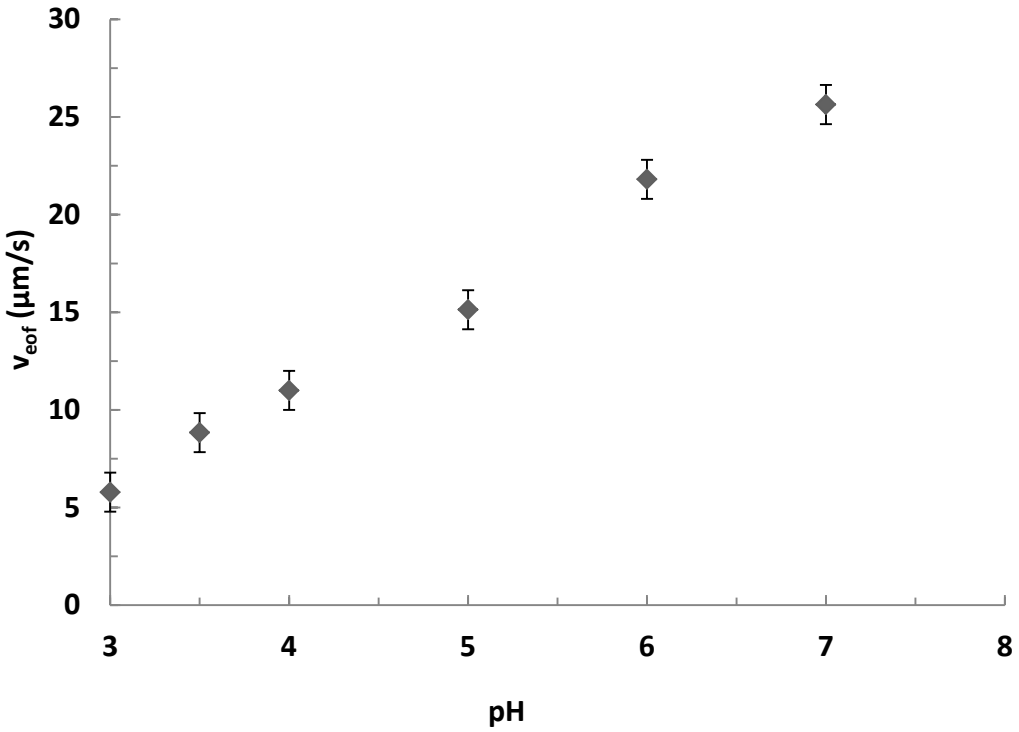

Figure 3-5.Plot of electroosmotic flow velocity vs. pH of permeate and feed solutions. *Applied current density was +15 mA/ cm^2.

From the data in Figure 3-5 we can calculate both the number density and pK_a of the surface acidic sites on the carbon nanotube membranes.[88] We apply the Boltzmann equation to first calculate the surface hydronium ion concentration ($[H^+]_s$) from the bulk solution hydronium ion concentration ($[H^+]_o$).

$$[\mathrm{H}^+]_s = [\mathrm{H}^+]_o \, exp\left(\frac{-e\zeta}{2kT}\right) \quad (3\text{-}11)$$

The zeta potential values needed at each pH can be obtained by utilizing Equation 3-7, employing the known values for the permittivity and viscosity of water (6.95 x10^{-10} C^2 J^{-1} m^{-1} and 0.890 cP)[89], and by measuring the resistivity of the electrolyte (2.27 kΩ cm). From the literature, Jimbo[88] determined the surface charge density is related to the number density of acidic sites (N_a) and the surface pK_a via Equation 3-12:

$$\sigma = -\left[\frac{(eN_a)}{(1+10^{pKa-pHs})}\right] \quad (3\text{-}12)$$

We solve Equation 3-9 for σ, and set it to equal Equation 3-12. By solving also for zeta potential using Equations 3-9 and 3-12, we derive Equation[90] 3-13.

$$\zeta = -\left[\frac{(eN_a)}{(1+10^{pKa-pHs})}\right]\left(\frac{\kappa^{-1}}{\epsilon}\right) \quad (3\text{-}13)$$

Zeta potential may be plotted against pH. and though beyond the scope of this thesis, a nonlinear least squares regression curve of Equation 3-13 with surface pKa and N_a as adjustable parameters can be used to obtain the number density and p*K*a of the surface acidic sites on the carbon nanotube membranes as described by Miller et al.[90, 88]

Conclusions

EOF is an important analytical phenomenon that can be used to elucidate information for a given system. This research has illustrated that the EOF rate and direction can be monitored and controlled across template-prepared carbon nanotube membranes through a variety of methods. EOF is proportional to the current density applied to a particular system. Thus the rate and direction of EOF can be controlled by changing the magnitude and the sign of the transmembrane current. The rate and direction of EOF can also be controlled by varying the pH of the contacting solution

phase at a constant applied current density. Ionic strength of the electrolyte solution and surface charge of the membrane play significant roles in EOF measurements.

In the future we hope to capitalize on the electronic conductivity of CNMs. We have previously shown that the sign and magnitude of the excess surface charge can be controlled potentiostatically in gold nanotube membranes by simply applying a potential to the membrane in an electrolyte solution.[91] We endeavor to control surface charge potentiostatically and simultaneously monitor EOF in CNMs. In this system we expect that the CNMs will exhibit excess negative surface charge when negative potentials are applied, and excess positive surface charge when positive potentials are applied.

CHAPTER 4
DISCUSSIONS AND CONCLUSIONS

Carbon nanotubes have attracted the interest of many scientists throughout the world. The strength, small dimensions and remarkable physical properties of carbon nanotubes have made them a material with a range of promising applications.

Many of these applications will require the use of uniform dense arrays of free-standing, open-ended nanotubes. One way to achieve such nanotubes is template synthesis. The Martin group and others have created template-synthesized carbon nanotubes by chemical vapor deposition of ethylene gas onto commercial alumina membranes. The key feature of template synthesis is that each carbon nanotube conforms to the pore morphology of the template membrane.

By utilizing this method carbon nanotubes can be grown with tailored properties, dimensions, and shapes. The goals of the research presented in this thesis were to customize the chemical, physical, and structural properties of carbon nanotube membranes and to study the fundamental transport processes occurring at the interface of the carbon nanotube membranes and the electrolyte by monitoring and controlling electroosmotic flow.

We have briefly introduced carbon nanotubes, their discovery, properties, the need for carbon nanotube membranes and some of the possible applications in which carbon nanotubes membranes may be utilized. One such possible application is as a new material for battery separators. A battery separator is a porous membrane placed between the anode and cathode of a battery. The main function of a separator is to keep the positive and negative electrodes apart in order to prevent electrical short circuits, while also allowing the transport of ionic charge carriers which are needed to

complete the circuit during the passage of current in an electrochemical cell. The most important requirements for Li-ion battery separators are permeability, porosity, chemical and thermal stability, pore size, and electrical resistance. Many of these characteristics are available and tunable in template prepared CNMs. We also explain in detail electroosmotic flow and the principles necessary to understand this phenomenon.

We detailed the utilization of the template method to fabricate carbon nanotube membranes. This method entails synthesis of carbon nanotube membranes by chemical- vapor deposition within the pores of alumina membrane templates with high pore density. We investigated and defined the growth rate of carbon on to alumina and discovered the necessary conditions for producing consistent, conductive, defect-free membranes.

We described the advantages of using the template method to customize nanostructures with specific characteristics. We illustrated methods of controlling certain parameters of chemical vapor deposition to produce and enhance different properties in the carbon nanotube membrane. Lastly, we discussed the methods of characterization for the CNM as they related to the specific aim of fluidic transport.

Electroosmotic flow is an important analytical phenomenon that can be used to elucidate information for a given system. The research in this thesis has illustrated that the EOF rate and direction can be monitored and controlled across template-prepared carbon nanotube membranes through a variety of methods.

The work presented here has been introductory in many ways. Much of this work has been a reproduction of previous studies [50, 58, 62, 81, 86] and has laid a necessary framework for new research frontiers. In the future we hope to capitalize on the

electronic conductivity of CNMs. We have previously shown that the sign and magnitude of the excess surface charge can be controlled potentiostatically in gold nanotube membranes by simply applying a potential to the membrane in an electrolyte solution.[91]

We endeavor to control surface charge potentiostatically and simultaneously monitor EOF in CNMs. In this system we expect that the CNMs will exhibit excess negative surface charge when negative potentials are applied, and excess positive surface charge when positive potentials are applied thus providing another avenue for controlling and modulating EOF.

LIST OF REFERENCES

(1) Tarascon, J. M.; Armand, M. Nature 2001, 414, 359-367.

(2) Winter, M.; Besenhard, J.O. Electrochim. Acta 1999, 45, 31-50.

(3) Nishi, Y. Lithium Ion Batteries, Wakihara, M.Yamamoto, O.,Eds.; Kodansha: Tokyo, Japan, 1998; pp 181.

(4) Hossain S. Handbook of Batteries, 2nd ed.;, Linden, D., Ed.; Mcgraw-Hill: New York; 1995; pp 12-35.

(5) Rand, D. A. J; Woods, R.; Dell R. M. Batteries for Electric Vehicles; Bagshaw, N. E., Ed.; Research Studies Press: Somerset, England 1998; pp 427.

(6) Choi, S.; Lim, H. Factors that affect cycle life and possible degradation mechanisms of lithium ion batteries based LiCoO2. J. Power Sources 2002, 111, 130-136

(7) Linden, D.; Reddy, T. B. Handbook of Batteries, 3rd ed.; McGraw-Hill: New York 2002.

(8) Besenhard, J. O., Ed. Handbook of Battery Materials; Wiley-VCH: Weinheim, Germany, 1999.

(9) Arora, P; Zhang, Z. Chem. Rev. 2004, 104, 4419-4462.

(10) Benett, J.; Choi, W. M. Developments in small cell separators. In Proceedings of the 10th Annual Battery Conference on Applications & Advances; IEEE: New York, 1995; p 265.

(11) Kinoshita, K.; Yeo, R. Survey on Separators for Electrochemical Systems; Lawrence Berkeley National Laboratory. January 1985.

(12) Berndt, D. Maintenance Free Batteries, 3rd ed., Research Studies Press: Somerset, England, 2003.

(13) Bode, H. Lead-Acid Batteries; John Wiley: New York, 1977.

(14) Falk, S. U.; Salkind, A. J. Alkaline Storage Batteries; John Wiley: New York, 1969.

(15) Fleischer, A.; Lander, J. J. Zinc-Silver Oxide Batteries; John Wiley: New York, 1971.

(16) Brodd, R. J., Friend, H. M., Nardi, J. C., Eds. Lithium Ion Battery Technology: ITE-JEC Press: Brunswick, OH, 1995.

(17) Wakihara, M., Yamamoto, O., Eds. Lithium Ion Batteries, Fundamentals and Performance; Wiley-VCH: New York, 1998.

(18) Yoshino, A. Chem. Ind. 1995, 146, 870.

(19) Schalkwijk, W. A. V., Ed. Advances in Lithium Ion Batteries; Kluwer Academic: New York, 2002

(20) Böhnstedt, W. Separators. In Handbook of Battery Materials; Besenhard, J. O., Ed.; Wiley-VCH: New York, 1999. pp 245-292

(21) Spotnitz, R. Separators for Lithium-Ion Batteries In Handbook of Battery Materials; Besenhard, J. O., Ed.; Wiley-VCH: New York 1999. pp 553–563

(22) Iijima, S. Nature 1991, 354, 56-58.

(23) Iijima, S.; Ichihashi, T. Nature 1993, 8, 3233-3250.

(24) Gao, G.; Cagin, T.; Goddard, W. A., III. Nanotechnology, 1998, 9, 183-191

(25) Yu, M.; Files, B. S.; Arepalli, S.; Ruoff, R.S. Phys. Rev. Lett. 2000, 84, 5552-5555.

(26) Hone, J.; Whitney, M.; Zettle, A. Synthetic Met. 1999, 103 2498-2499.

(27) Odom, T.W.; Huang, J.; Kim, P.; Lieber, C. M; Nature 1998, 391, 62-64.

(28) Satishkumar, B.C.; Govindaraj, A.; Sen, R.; Rao, C.N.R. Chem. Phys. Lett, 1998, 293, 47-52.

(29) Frank, S.; Poncharal, P.; Wang, Z.L.; Science 1998, 280, 1744-1746

(30) Thess, A.; Lee, R.; Nikolaev, P.; Dai, H.; Petit, P.; Robert, J.; Xu, C.; Lee Y. H.; Kim, S. G.; Rinzler, A. G.; Colbert, D. T.; Scuseria G.; Tománek, D.; Fischer, J. E.; Smalley, R. E. Science 1996, 273, 483-487.

(31) Ebbesen, T.W.; Ajayan P.M. Nature 1992, 358, 220-222

(32) Lange, H.; Huczko, A.; Byszewski, P.; Mizera E.; Shinohara, H. Chem. Phys. Lett. 1998 289, 174-180.

(33) Chernozatonskii, L.A.; Kosakovskaya, Z.Y.; Fedorov, E.A.; Panov, V.I. Phys. Lett. A 1995, 197, 40-46.

(34) Ge, M.; Sattler, K. Science 1993, 260, 515-518.

(35) Ge, M.; Sattler, K. Appl. Phys. Lett. 1994 64, 710-711.

(36) Dai, H. Accounts of Chemical Research 2002, 35, 1035-1044

(37) Baughman, R. H.; Zakhidov, A.; de Heer, W. A. Science 2002, 297 787-792.

(38) Campbell, S.A. The Science and Engineering of Microelectronic Fabrication; Oxford University Press: Oxford U.K., 1996.

(39) Dai, H Sur. Sci. 2002, 500, 218-241.

(40) Fan, S.S.; Chapline, M.G.; Franklin, N. R.; Tombler, T. W.; Cassell, A.M.; Dai, H. J. Science 1999, 283, 512-514.

(41) Teo, K. B. K.; Chhowalla, M.; Amaratunga, G.A.J.; Milne, W. I.; Hasko, D. G.; Pirio, G.; Legagneux, P.; Wyczisk, F.; Pribat, D. Appl. Phys. Lett. 2001, 79, 1534-1536.

(42) Franklin, N. R.; Dai, H. J. Adv. Mater. 2000, 12, 890-894.

(43) Cassell, A.M; Franklin, N.R.; Tombler, T.W.; Chan, E.M.; Han, J.; Dai, H. J. J. Am. Chem. Soc. 1999, 121, 7975-7976.

(44) Zhang, Y.G.; Chang, A.L.; Cao, J.; Wang, Q.; Kim, W.; Li Y. M.,; Morris, N.; Yenilmez, E.; Kong, J.; Dai, H. J. Appl. Phys. Lett. 2001, 79, 3155-3157.

(45) Hulteen, J.C.; Martin, C.R. J. Mater. Chem. 1997, 7, 1075-1087.

(46) Martin, C. R. Science 1994, 266, 1961-1966.

(47) Martin, C. R.; Mitchell, D. T. Anal. Chem. 1998, 70, 322A-327A.

(48) Che, G.; Lakshmi, B. B.; Fisher, E. R.; Martin, C. R. Nature 1998, 393, 346-349.

(49) Kyotani, T.; Tsai, L. F; Tomita, A. Chem.Matter. 1996, 8, 2109-2113.

(50) Miller, S. A.; Young, V. Y.; Martin, C.R. J. Am. Chem. Soc. 2001, 123, 12335-12342.

(51) Che, G. Lakshmi, B. B.; Martin, C. R.; Fisher, E. R.; Ruoff, R.S. Chem. Mater. 1998, 10, 269-267.

(52) Kyotani, T.; Tsai, L. F.;Tominta, A. Chem. Commun. 1997, 701-702.

(53) Penner, R.M.; Martin, C.R. Anal Chem. 1987, 59, 2625-2630.

(54) Cheng, I. F.; Martin, C. R. Anal. Chem. 1988, 60, 2163-2165.

(55) Possin, G.E. Rev. Sci. Instrum. 1970, 41, 772-774

(56) Huczko, A, Appl. Phys A-Mater. 2000, 70, 365-376.

(57) Martin, C. R. Accounts of Chemical Research 1995, 28, 61-68

(58) Wirtz, M.; Miller, S. A.; Martin, C. R. Int. J. Nanosci. Ser. 2002, 1, 255-268.

(59) Liang, Z.; Susha, A. S.; Caruso, F. Adv. Mater. 2003, 15, 1849-1853.

(60) Perry, J.L.; Martin, C. R.; Stewart, J. D. Chem.- Eur. J. 2011, 17, 6296-6302.

(61) Pan, L.; Qiu, H.; Dou, C.; Li, Y.; Pu, L.; Xu, J.; Shi, Y. Int. J. Mol. Sci. 2010, 11, 2636-2657.

(62) Miller, S.A.; Martin, C. R. Carbon Nanotubes: Electroosmotic Flow Control in Membranes. In Dekker Encyclopedia of Nanoscience and Nanotechnology 1st ed.; Schwarz, J. A., Contescu, C. K. P., Eds.; Marcel Dekker, Inc: New York. 2004; pp 519-528.

(63) Probstein, R.F. Physicochemical Hydrodynamics: An Introduction. Wiley: New York, 1994.

(64) Shaw, D. Introduction to Colloid and Surface Chemistry: 3rd ed.; Butterworth: Boston, Mass., 1980.

(65) Reuss, F. F. Proceedings of the Imperialist Society of Naturalists of Moscow 1809, 3,327-344.

(66) Zhu, W.; Bower, C.; Kochanski, G.; Jin, S. Appl. Phys. Lett. 1999, 75, 873-875.

(67) Bachtold, A.; Hadley, P.; Nakanishi, T.; Dekker, C. Science, 2001, 294, 1317-1320.

(68) Frankland, S. J. V.; Caglar, A.; Brenner, D.W.; Griebel, M. J. Phys. Chem. B. 2002, 106, 3046-3048.

(69) Darkrim, L. F.; Malbrunot, P.; Tartaglia, G.P. Int. J. Hydrogen Energ. 2002, 27, 193-202.

(70) Dillon, A. C.; Heben, M. J. Appl. Phys. A-Mater. 2001, 72, 133-142.

(71) Poirier, E.; Chahine, R.; Bénard, P.; Cossement, D.; Lafi, L. Appl. Phys. A-Mater. 2004, 78, 961-967.

(72) Wang, Q.; Challa, S. R.; Sholl, D.S.; Johnson, J.K. Phys. Rev. Lett. 1999, 82, 956-959.

(73) Baddour, C.E.; Briens, C. Int. J. Chem. React. Eng. 2005, 3, p. R3.

(74) Koros, W. Chem. Eng. Prog. 1995, 91, 68.

(75) Sun, L.; Crooks, R. M. J. Am. Chem. Soc. 2000, 122, 12340-12345.

(76) Smits, F. M. *Bell Syst. Tech. J.* **1958,** *5* 711-718

(77) Valdes, L. G. *Proc. I.R..* . **1954,** 42, 420-427.

(78) Crawford, G. P.; Steele, L. M.; Ondriscrawford, R.; Iannacchione,G. S.; Yeager, C. J.; Doane, J. W.; Finotello, D. J. Chem Phys. 1992, 96, 7788-7796.

(79) Morosanu, C. E. Thin Films by Chemical Vapour Deposition; Elsevier: Amsterdam, 1990; 7.

(80) Choi, J. Developments in small cell separators. In Proceedings of the 10th Annual Battery Conference on Applications & Advances; IEEE: New York, 1995; p 265.

(81) Bath, B. D.; Lee, R. D.; White, H. S.; Scott, E. R. Anal. Chem. 1998, 70, 1047-1058.

(82) Bath, B. D.; White, H. S.; Scott, E. R. Anal. Chem. 2000, 72, 433-442.

(83) Miller, S. A.; Martin, C. R. J. Am. Chem. Soc. 2004, 126, 6226-6227.

(84) Srinivasan, V.; Higuchi, W. I. Int. J. Pharm. 1990, 60, 133-138.

(85) Panzer, R. E.; Elving, P. J. Electrochim. Acta 1975, 20, 635-647.

(86) Bismarck, A.; Springer, J. Colloids Surf. A: Physicochem. Eng. Asp. 1999, 159, 331-339.

(87) Garcia, A. B.; Cuesta, A.; Montes-Moran, M. A.; Martinez-Alonso, A.; Tascon, J. M. D. J. Colloid Interface Sci. 1997, 192, 363-367.

(88) Jimbo, T.; Tanioka, A.; Minoura, N. *Langmuir* **1998**, 14, 7112-7118.

(89) Weast, R. C.; Astle, M. J.; Beyer, W. H., Eds. *CRC Handbook of Chemistry and Physics*, 66th ed.; CRC Press, Inc.: Boca Raton, FL, 1985.

(90) Miller, S.A. Nanofludics in Tailored Carbon Nanotube Membranes. Ph. D. Dissertation, University of Florida, U. S., May 2011.

(91) Nishizawa, M.; Menon, V. P.; Martin, C. R. Science 1995, 268, 700-702.

BIOGRAPHICAL SKETCH

William Cornelius Hardy was born in Jackson, MS. He graduated from Jackson State University in 2007 with a B.S. in chemistry and 2008 with a M.S in chemistry. While attending JSU, William discovered he had a passion for nanoscience. After graduating, from JSU, William continued his education by joining the research group of Dr. Charles R. Martin at the University of Florida in August 2008. In his free time William enjoys music, reading, and cooking.